

Synthesis of alkyl-branched fatty acids by isomerization on micro-mesoporous ferrierite-based zeolitic materials

Jonathan Fabian Sierra-Cantor^{a,1}, Olinda Gimello^a, Carlos-Alberto Guerrero-Fajardo^b,
Francesco Di Renzo^a, Hugo Petitjean^a, Maxime Riviere^{a,2}, Corine Gérardin^{a,*},
Nathalie Tanchoux^{a,*}

^a Institut Charles Gerhardt, Université de Montpellier, CNRS, ENSCM, Montpellier, France

^b Department of Chemistry, Universidad Nacional de Colombia, Aprovechamiento Energético de Recursos Naturales, Carrera 30 45-03, Bogotá, Colombia

ARTICLE INFO

Keywords:

Hierarchically porous ferrierite

Fatty acids isomerization

Continuous flow process

Reaction mechanism

Catalyst deactivation

ABSTRACT

The synthesis of alkyl-branched fatty acid methyl esters from fatty acids is of great interest to synthesize high value-added products. The isomerization reaction catalyzed by microporous zeolites is promising due to its high yields, but rapid deactivation is its main drawback. In this work, a microporous ferrierite synthesized by a well-controlled alkaline recrystallization process, was evaluated as a catalyst in the isomerization of methyl oleate. Recrystallized materials present improved accessibility of acid sites at the mouth of 10-MR pores due to the increase of the mesopore surface. Methyl oleate isomerization has been implemented in batch conditions and in a continuous flow process with experiments lasting more than 3 days. Stable yield of branched isomers higher than 50% was reached at 285 °C and 3.5 h⁻¹ WHSV. The catalytic results, combined with a detailed analysis of fresh and spent catalysts, has provided information on the phenomena involved, in particular deactivation.

1. Introduction

Interest in lipid biomass as a renewable substitute for fossil oil supply has increased in recent years [1,2]. Among them, the production of vegetable oils increased by 40% between 2010 and 2020, reaching values around 208 Mt/year [3], with a further increase of more than 20% expected in the coming years [4]. Although about 77% of these oils are used for food production, biofuels, and oleochemical production represent an important part of this demand [4]. In addition to their general uses, they have been used to produce biofuels and other high-value oleochemical products [5]. They have been identified as precursors of high-value products such as biodegradable and biosafe fungicides, surfactants, monomers, plasticizer additives, cosmetics, personal care products, lubricants, etc [1,4–6].

In this context, different routes have been investigated for obtaining biodiesel [7], renewable diesel [8], or biolubricants [5] from vegetable oils [9] using porous acidic materials as catalysts [10]. Among them, the isomerization of fatty acids to branched chain fatty acids has attracted

attention in recent years. It has resulted in obtaining branched molecules with improved physicochemical properties [11,12]: higher solubility, better water tolerance, oxidative stability [13], lower melting/freezing points, lower viscosity as well as good spreadability, among others [5,14–18]. With this in mind, they have been used as limiting additives in biodegradable lubricants [5,19], as emollients in personal care products [14,20,21], and more recently as additives to improve the cold flow properties of biodiesel [22–24].

These alkyl-branched fatty acids are obtained by the isomerization reaction, a complex reaction (see Fig. 1), which can lead to rapid deactivation of the porous acidic catalyst. This reaction is mediated by the rearrangement of a carbenium ion. This step is followed by a skeletal rearrangement in which chain propagation of the carbenium ion onto the hydrocarbon chain of the fatty acid moiety can form multiple double bond positional isomers, cis/trans isomers as well as positional isomers of the branched monoalkyl molecules [23]. In addition, under these pressure and temperature conditions, a large number of by-products can be formed, such as hydroxylated and saturated fatty acids, gamma, and

* Correspondence to: ICGM, Pôle Chimie Balard Recherche, 1919 route de Mende, 34293 Montpellier Cedex 5, France.

E-mail addresses: corine.gerardin@enscm.fr (C. Gérardin), nathalie.tanchoux@enscm.fr (N. Tanchoux).

¹ Present address of J.F. Sierra Cantor: Institut de Chimie des Milieux et Matériaux de Poitiers (IC2MP), Université de Poitiers, CNRS, UMR 7285, 4 Rue Michel Brunet, TSA 51106, F-86073 Poitiers 9, France.

² Present address of M. Rivière: VINCI TECHNOLOGIES, 27B Rue du Port - Parc de l'île, 92022 Nanterre.

delta lactones, oligomers such as dimers or estolides, as well as products from catalytic cracking [21,25,26]. On the other hand, under these reaction conditions, catalytic β -scission cracking [27] leads to the formation of alkylbenzenes [25] and consequently, it can lead to the formation of carbonaceous deposits formation, which cannot desorb from the active sites, blocking the pores and ultimately deactivating the catalyst [12,25].

With this in mind, several acid porous materials have been tested as catalysts for this reaction [28], materials such as clays (montmorillonite [14,29]), sulfated zirconia with metal promoters, acidic alumina supported noble metals, silica supported phosphotungstic heteropolyacids [30]; and more recently aluminosilicates and silicoaluminophosphates [5,15]. Among them, zeolites have shown a breakthrough performance. Although zeolites with large pores such as mordenite (yield: 66.5% [31]) [32], zeolite L (yield: 51% [33]), and β -zeolite (yield: 50% [23,34,35]) have been tested, the real breakthrough came from the use of a zeolite with smaller pore size, ferrierite. Yields up to 74% in branched chain fatty acids were obtained [15,21,31,36]. It was observed that this particular catalytic performance of the zeolites is caused mainly by well-constrained porous network in their ordered structure. The observed high yields were explained by the induced shape selectivity, which limits mainly the oligomerization reactions. The work of Ngo and coworkers showed that the distribution of products depends on the architecture of the channels and the nature of the acidic sites of the zeolites [15,21,31]. However, this well-constrained microporous network leads to a faster loss of catalytic activity of the ferrierite catalysts by coke formation. This is an important drawback for the implementation of zeolite-based catalyst processes for the production of branched chain fatty acids. Various alternatives have been studied to improve catalytic performance of zeolites. The yield of branched chain fatty acids was improved to 87% using bulky Lewis bases as additives [25,30]. Treatments with magnesium salts were shown to further reduce the formation of dimers during the reaction [36]. Recently, the presence of intracrystalline mesopores in ferrierite structures has been shown to

significantly improve the catalytic performance of the isomerization reaction [37–40].

Considering that the presence of these intracrystalline mesopores could help to avoid the losses in their catalytic performance in the isomerization reaction of fatty acids [41,42], this work has analyzed the use of a zeolite with intracrystalline mesopores, previously developed in our research group [43], as a catalyst in this reaction. Considering that this meets the specifications previously described to carry out isomerization reaction on fatty acids, in this work, its performance was compared to parent exchanged ferrierite in methyl oleate isomerization. Their catalytic performance in different conditions of pressure and temperature was compared on a batch and a downstream fixed bed continuous flow reactor to evaluate the effect of the intracrystalline mesopores on the parameters of conversion, selectivity, and time-on-stream stability.

2. Experimental section

2.1. Reagents and materials

Reagent grade oleic acid (91.6%wt. C18:1; 3.7% wt. C18:2; 2.6% wt. C18:0; 1.4% wt. C16:0; 0.7% wt. other), sulfuric acid 98%, sodium hydroxide, cetyl Trimethyl Ammonium Bromide (CTAB), heptane, methyl arachidate, and methanol were purchased from Sigma-Aldrich. Na, K-ferrierite (HSZ-720 KOA® Si/Al: 9.2) was purchased from Tosoh Corp.

Methyl Oleate was synthesized by acid esterification under reflux at 60 °C for 3 h with 2% H₂SO₄ and a 6:1 molar ratio of oleic acid to methanol. The product was purified by successive washings with water at 40 °C followed by vacuum distillation at 60 °C. The purity of the methyl esters was checked (ASTM D664) and the content of free fatty acids was lower than 1%.

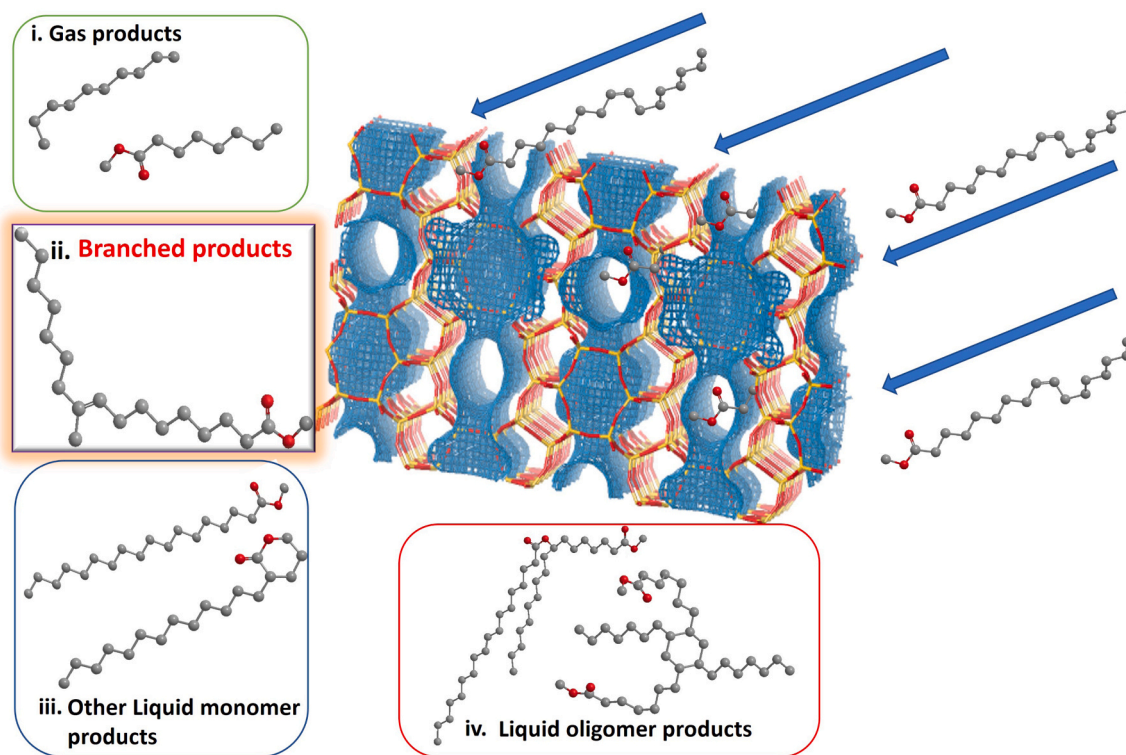


Fig. 1. Reaction of isomerization unsaturated fatty acid methyl esters on porous acid materials: (i.) gas products like light alkanes and volatile fatty acids, (ii.) branched fatty acid methyl esters, (iii.) other liquid monomer products like straight saturated and unsaturated fatty acid methyl esters, gamma and delta lactones, (iv.) Liquid oligomer products such as estolides and dimers.

2.2. Zeolite materials recrystallization and characterization

In a typical synthesis, following the methodology of Cheng *et al.* [43], 4.89 g of Na, K–Ferrierite, and 2.49 g of CTAB were mixed with 150 mL of 0.2 M NaOH solution. After stirring for 30 min, the suspension was hydrothermally treated at 130 °C in a Teflon-lined stainless-steel autoclave for 72 h. After cooling, the solid was filtered and washed with deionized water until to get pH 7. The product was then dried overnight at 80 °C, it was ground, and subjected to ion exchange in 150 mL of a 1.0 M NH_4NO_3 solution for six hours at room temperature. The solid was then filtered, washed, and dried. Later, this NH_4 -form ferrierite with CTAB was calcined in an air flow (200 mL/min) in a tube furnace with the following heating program: from room temperature to 550 °C with a heating ramp of 120 °C/h and a plateau of sixteen hours. The recrystallized ferrierite in the H-form (H-FER-REC) was obtained (mass yield: 65.4%). On the other hand, the ion exchange, drying, and calcination steps were carried out under the same conditions directly on Na, K–Ferrierite to obtain the H-form of the parent zeolite (H-FER-PAR) or simply referred to hereafter as the parent ferrierite.

On the one hand, the characterization of the fresh catalyst was as follows. The characterization of the structure, porosity, and composition in these ferrierite materials was carried out according to the characterization methodology of Cheng *et al.* [43]. The crystal structure was analyzed by powder X-ray diffraction (XRD). Data were recorded by continuous scanning in the range of 2θ values of 0.5–6° and 4–50°. Surface areas and pore volumes were calculated from the analysis of nitrogen adsorption-desorption isotherms recorded at 77 K using a Micromeritics TriStar 3000. The compositions of the samples were determined by elemental analysis using the energy dispersive X-ray (EDS) analysis method on a SEM FEI QUANTA 200 F with an accelerating voltage of 15 kV (PT MEA-UM). The particle size and morphology of the materials were evaluated using a SEM HITACHI 4800 S (PT IEM) with an accelerating voltage of 5 kV. The distribution, size, and orientation of the intracrystalline mesopores were determined by transmission electron microscopy (TEM) using a JEOL 1200–1400 Plus EXII electron microscope with an accelerating voltage of 100 kV (PT MEA-UM). In addition, ^{29}Si and ^{27}Al Magic Angle Spinning Nuclear Magnetic Resonance (MAS NMR) analysis of the zeolitic materials was performed on a 300 MHz Varian VNMR300 spectrometer (UM) using a Varian T3 MAS probe with 7.5 mm ZrO_2 rotors. The ^{29}Si MAS NMR spectra were acquired using the quantitative Single Pulse technique with ^1H decoupling with a recycle delay of 60 s, a $\pi/6$ pulse of 2 μs , and a spin rate of 5 kHz. Q8M8H (octakis(dimethylsiloxy)octasilsesquioxane) was used as a secondary reference (left peak at –2.25 ppm). The spectral window width is 50 kHz and the line broadening is 50 Hz. ^{27}Al MAS NMR spectra were acquired using the quantitative Single Pulse technique with ^1H decoupling with a recycle delay of 1 s, a $\pi/6$ pulse of 2 μs , and a spinning rate of 22 kHz. Aluminum nitrate was used as a secondary reference (peak at 0.0 ppm). The spectral window width is 192 kHz and the line broadening is 50 Hz. Acidic site characterization was performed by temperature programmed desorption of ammonia (TPD- NH_3) to determine the total number of acidic sites and by the infrared analysis of adsorption/desorption analysis of acetonitrile to analyze the different acidic sites. TPD- NH_3 was performed on a Micromeritics AutoChem II® apparatus. Solids (30–50 mg) were calcined in air up to 550 °C, cooled down to 100 °C, and saturated with ammonia. The physisorbed base was swept in a He flow (50 mL/min, 2 h) while the chemisorbed ammonia was desorbed by increasing the temperature (10 °C/min) up to 700 °C. Finally, infrared (IR) spectra were recorded on a Bruker EQUINOX 55 spectrometer with a DTGS detector in transmission mode. All the IR analyses were performed at room temperature. Infrared analysis of adsorbed CD_3CN (Aldrich, 99.8% D atoms) was performed in a low pressure quartz transmission cell with KBr windows. The catalyst was pressed into a self-supporting wafer (5000 kg·cm^{–2}, 30 mg, 18 mm in diameter) and then pretreated in the IR cell under a dynamic vacuum (10^{–5} mbar) at 250 °C for 16 h before cooling down to room

temperature. Deuterated acetonitrile was then adsorbed on the catalyst at an equilibrium pressure of 1.0 mbar. It was then desorbed under a dynamic vacuum for three hours. Four desorption temperatures (25, 50, 100, and 150 °C) were investigated by increasing the temperature of the catalyst wafer temperature for 15 min. After each desorption treatment, the catalyst was cooled to room temperature before IR measurement. Band areas were computed using Fityk software. The molar density of acid sites was calculated using the Beer-Lambert law and extinction coefficients of 3.60 cm²·μmol^{–1} for Lewis acid sites (2321 cm^{–1}) and 2.05 cm²·μmol^{–1} for Brönsted acid sites (2306–2275 cm^{–1}) [44].

On the other hand, the analysis of the washed spent catalytic materials was performed after the removal of soluble impurities. Each stored spent catalytic material (0.5 g) was washed with 10 mL of acetone, centrifuged, and dried at 60 °C. A 24-hour Soxhlet treatment with dichloromethane was then performed. The total amount of coke in each sample was determined by thermal gravimetry (TG) using a PerkinElmer TGA 4000. Analyses were performed from 40 °C to 900 °C with a ramp of 5 °C/min in air flow (60 mL/min). The amount of coke was calculated as the sum of mass losses from 250 to 700 °C. On the other hand, ^{13}C Cross-Polarization Magic Angle Spinning (CP MAS) NMR analysis was performed on these spent catalytic materials. The spectra were acquired on a 300 MHz Varian VNMR300® spectrometer ("Wide Bore" magnet at 7.05 Tesla). A Varian T3 MAS probe was used with 3.2 mm zirconia rotors and a spinning speed of 12 kHz. Spectra were acquired using the CPMAS technique with a recycle delay of 3 s, a $\pi/2$ pulse of 5 μs , and a contact time of 0.5 ms. The spectral window width was 50 kHz, the acquisition time was 40 ms and the line broadening was 50 Hz. Adamantane was used as a secondary reference (left peak at 38.5 ppm).

2.3. Catalytic tests

Isomerization of methyl oleate in batch conditions was carried out with a catalyst loading of 5% wt., under a N_2 atmosphere, with a reaction time of eight hours, working at temperatures between 260 and 285 °C and pressures between 2.0 and 4.0 MPa in a 200 mL flange autoclave. The catalytic material (see Section 2.2) containing particles of size < 250 μm was prepared by compressing the powder at 196 MPa, crushing, and sieving it to the desired size. In a typical experiment, 50 g of methyl oleate and 2.5 g of the catalytic material were placed in the autoclave and then heated to the desired temperature, which was considered as the starting point of the reaction. After the reaction, the system was cooled down to room temperature and the gas outlet valve was opened to collect gas samples in a cryotrap. After opening the reactor, the reaction mixture was removed and filtered at room temperature. The liquid fraction was sent for GC analyses. The spent catalysts were characterized as described above. The liquid phase extracted from the two washings with acetone and dichloromethane was analyzed by GC-MS and MALDI-TOF.

The isomerization of methyl oleate under continuous flow conditions was carried out in a downstream fixed bed continuous flow reactor (6 mm ID) using 1–1.3 g of catalytic material (see Section 2.2) with a particle size in the range of 250 to 425 μm prepared as described above, and mixed with quartz with a particle size ranging in the range of 150 to 250 μm . The amount of quartz was adjusted to keep the total volume of the catalytic bed constant at 3.7 cm³. The catalyst was activated in situ under a 50 mL/min hydrogen flow at 400 °C for 18 h (heating rate: 120 °C/h). Methyl oleate was pumped at a flow rate of 4.0 mL/h, allowing a W.H.S.V. of 3.5 h^{–1} in the reactor and mixed with the carrier gas (N_2) at the desired pressure (between 2.0 and 4.0 MPa). The reaction temperature varied between 260 and 325 °C during the course of a reaction. Lighter gaseous reaction products were analyzed on-line by GC, while liquid fractions were periodically collected for separate analysis (see Section 2.4). If the experiment lasted more than one day, the starting material flow was reduced to allow a WHSV of 1.2 h^{–1} at night. The next day, the flow was normalized to the previous conditions, and the new temperature condition was fixed. This procedure was repeated

every day during the course of a typical experiment.

2.4. Analytical method

The products of methyl oleate isomerization form a complex mixture of compounds in the gas and liquid phases due to the complexity of the reaction.

The gas fraction products of methyl oleate isomerization were analyzed using a gas chromatograph GC equipped with an FID detector (Agilent 7890 A). The chromatographic separation was performed on an Rt-Q-Bond Plot capillary column (30 m x 0.25 mm x 8 µm) coupled in series with an HP-5-ms capillary column (30 m x 0.25 mm x 0.25 µm), with hydrogen as the carrier gas.

The liquid fraction was analyzed by two different GC methods. For both analyses, samples were prepared by mixing 10 µL of the liquid phase products with 50 µL of internal standard solution (methyl arachidate) and diluting in 1.0 mL of heptane. 1.0 µL of this mixture was injected. The first type of GC analysis was used to determine the amount of oligomers in the samples. The products were analyzed on a GC (Varian 3900) equipped with an HP-5HT® capillary column (15 m x 0.32 mm x 0.10 µm). In the second method, all compounds in the liquid fraction (except oligomers) were identified and quantified. Samples were prepared as previously described, and the analysis was performed using a gas chromatograph coupled to a GC-MS mass spectrometer (Shimadzu QP-2010plus). Chromatographic separation was performed on a ZB-FAMES® capillary column (60 m x 0.25 mm x 0.20 µm).

The conversion (C) was defined as $C = 100 \left(1 - \frac{Q_{in-t}}{Q_{in-0}} \right)$ where Q_{in-t} is the concentration of the remaining substrate i at a time t , and Q_{in-0} is the initial concentration of the substrate in the starting material. Due to the considerable complexity of the products, they are classified into different families of products in the liquid phase: branched C18 isomer products, linear saturated FAME products (methyl stearate), straight C18 isomers of methyl oleate, cracking products, oligomer, and other products. The yield of a j family of compounds (Y_j) is defined as: $Y_j = 100 \left(\frac{Q_{j-t}}{Q_{in-0}} \right)$ where Q_{j-t} is the concentration of the j kind of compound and Q_{in-0} is the concentration of the substrate in the starting material.

Oligomers were qualitatively analyzed in the liquid fraction products by MALDI-TOF MS and MS/MS analyses. In addition, the dichloromethane liquid extracts from the Soxhlet procedures of washing of the spent catalysts were also analyzed by the same method. The samples were dissolved in dichloromethane at 5 mg/mL. The matrix used was DHB (2,5-dihydroxybenzoic acid) dissolved at 10 mg/mL in acetone. The cationizing agent was lithium chloride (5 mg/mL in acetone). First, 1 µL of LiCl solution was applied to the MALDI plate followed by 0.5 µL of matrix and 0.5 µL of the sample solution. The plate was allowed to dry before analysis. Full scan mass spectra and MS/MS spectra were performed on a Bruker Rapiflex MALDI-TOF/TOF using a nitrogen laser for MALDI ($\lambda = 337$ nm). All spectra were acquired in positive ionization mode. Mass spectra from 3000 shots were accumulated for spectra at a 25 kV acceleration voltage and reflectron lens potentials at 26.3 kV. A mixture of peptides was used for external calibration. For the MS/MS mode, the transmission of precursor ions in the collision cell was optimized using an 18 kV deceleration lens and a 2.9 kV MS/MS Pulse.

Finally, the GC-MS chromatographic analysis of the liquid extracts from spent catalytic materials was performed using the same instrument equipped with an HP-5-ms capillary column (30 m x 0.25 mm x 0.25 µm). Each liquid extract was diluted to 1.0 mL of the appropriate solvent (acetone & dichloromethane).

3. Results and discussion

3.1. Zeolite Materials recrystallization and characterization

Using the recrystallization conditions for highly stable low silica ferrierite established by Cheng *et al.* [43], it was possible to produce a ferrierite-based material that had an added mesopore system and retains its crystalline structure and micropores.

Fig. 2 shows the XRD patterns of the parent and recrystallized ferrierite materials. Although both show diffraction peaks typical of highly crystalline ferrierite, the recrystallized material shows less intense and broader peaks; reflecting a loss of crystallinity and the shortening of coherent diffraction domains by the formation of mesopores [43] during recrystallization. No peaks are observed in the small angle scattering region, indicating the absence of an ordered mesopore structure. On the other hand, no other crystalline phase (SOD, GIS) or lamellar material was formed; such phases have been previously reported when CTAB has not been used in the recrystallization [43].

The transmission electron microscopy (TEM) micrographs of the H-form ferrierite-based zeolitic materials along the [001] and [100] planes are shown in Fig. 3. On the one hand, the H-FER-PAR has platelet-like crystals with very few small pores (Fig. 3-A1), which were not previously observed in parent Na,K-Ferrierite [43], certainly due to the demetallation process occurring during ion exchange. A slight increase in the Si/Al ratio from 9.2 in Na,K-FER to 9.7 in H-FER-PAR confirmed this (see Table 1). On the other hand, TEM images of H-FER-REC show a large number of parallelepiped mesopores with blunt edges (Fig. 3-B1). There is a wide distribution of quasi-square mesopores with pore sizes ranging from 10 to 50 nm in the [010] and [001] directions. Some larger pores are rectangular in shape with length greater than 100 nm. They may be the result of merging of adjacent pores. According to Fig. 3-B2, the mesopores have a thickness from 1.5 to 20 nm. Comparing Fig. 3-B1 and Fig. 3-B2, it can be seen that the flat mesopores are parallel to the [100] platelet faces of the crystals and are located in different layers from the surface to the interior of the crystals. TEM images allowing a statistics of crystal size (see Fig S1) showed that the thickness of the FER crystals in the [100] direction appeared to be smaller, less than 0.3 µm, in the recrystallized material than in the parent H-form material, where more platelets with a thickness greater than 0.4 µm are observed. This suggests that the extension of the flat mesopores can sometimes lead to a delamination of the ferrierite crystals.

According to the information summarized in Table 1, an increase in the volume of intracrystalline mesopores from 0.01 in H-FER-PAR to 0.13 cm³/g in the recrystallized material, as well as in the volume of intercrystalline mesopores from 0.06 to 0.11 cm³/g, confirms the presence of a new system of mesopores. The surface area of the mesopores increased from 18 to 76 m²/g. The presence of a large hysteresis loop in the N₂ sorption isotherms of H-FER-REC (see Fig. 4), in contrast to the isotherms of the parent FER, confirms the presence of large mesopores, as previously reported by Cheng *et al.* [43]. The sharp desorption by cavitation at p/p^0 0.45 indicates that the mesopores are connected to the outer surface of the crystals by openings smaller than 4 nm, quite likely the structural microporosity of the zeolite. Although the surface area increased only slightly from 379 to 406 m²/g, and the micropore volume decreased slightly from 0.13 to 0.10 cm³/g, the outer surface area increased significantly from 21 to 82 m²/g. This is consistent with the smaller size of the recrystallized ferrierite crystals compared to that of the parent ferrierite, as observed in the SEM images (Fig. 5) and also clearly seen in the TEM images (Fig S1).

On the other hand, the Si/Al ratio decreased significantly from 9.7 to 6.6 in the parent and recrystallized samples, respectively, due to the desilication process promoted by the base attack. Considering this change in Si/Al ratio, it may indicate that the recrystallization mechanism does not correspond to the mechanism proposed by Ivanova *et al.* [45] for two-step recrystallization, where the Si/Al ratio does not change during recrystallization. On the other hand, the behavior of this

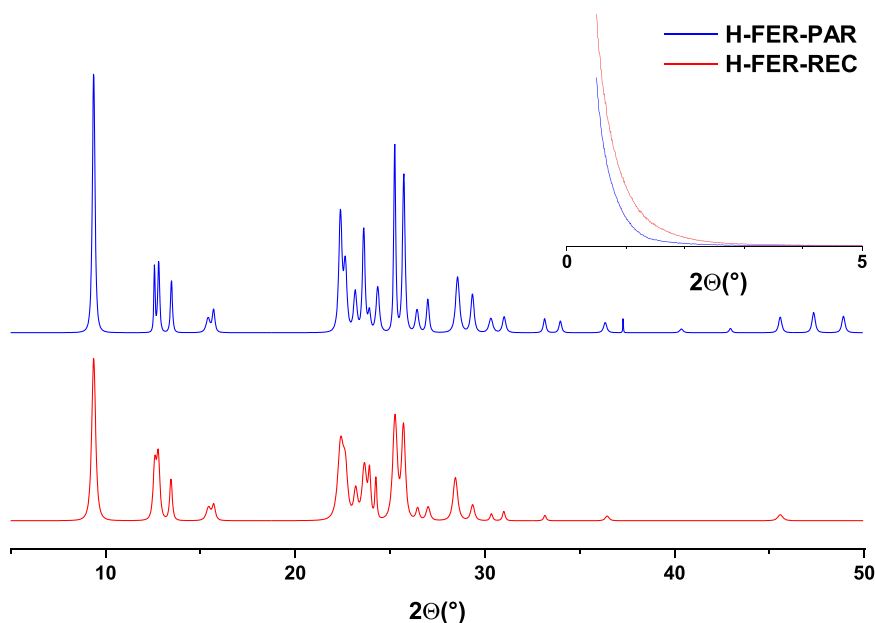


Fig. 2. Powder X-ray diffraction patterns of parent (in blue) and recrystallized (in red) ferrierite materials with magnification of small angle patterns of 0.5–5 ° of powder X-ray diffraction patterns of parent (H-FER-PAR) and recrystallized (H-FER-REC) ferrierite materials.

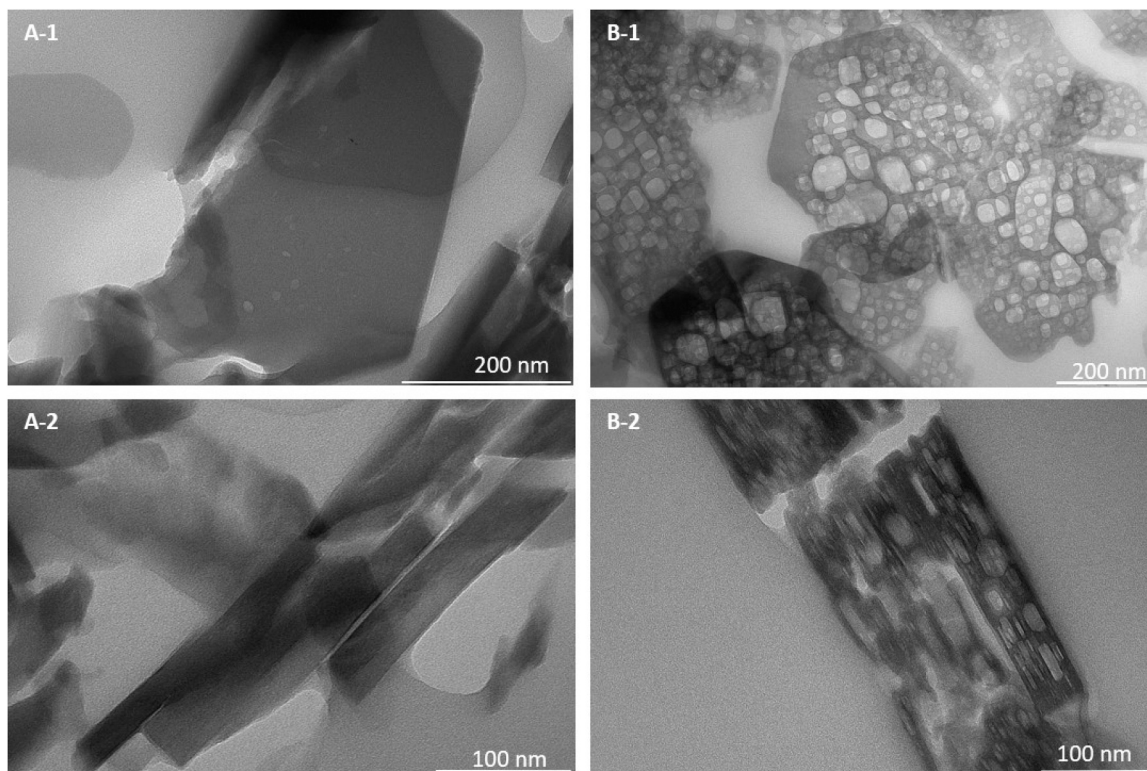


Fig. 3. TEM images of ferrierite materials (1) oriented on [100] (200 nm scale bars), and (2) oriented on [010] (100 nm scale bars). A. Parent Ferrierite (H-FER-PAR). B. Recrystallized Ferrierite (H-FER-REC).

one-step recrystallization can be better explained by the crystal rearrangement mechanism proposed by García-Martínez and coworkers. [46]. As observed by ammonia temperature programmed desorption (TPD-NH₃) analysis (Fig S2), the most important change from H-FER-PAR to H-FER-REC was the decrease of the peak corresponding to the strong acidity. Minor changes were observed in the maximum peak temperature and total area related to the total acidity of the samples.

The significantly higher amount of aluminum in the recrystallized ferrierite did not lead to an increase in acidity. In fact, the total acidity decreased from 1050 μmol/g in H-FER-PAR to 720 μmol/g in H-FER-REC with a larger proportion of the strongest acidic sites. This may be related to the partial destruction of the microporous crystal structure during the desilication process [47].

To confirm this solid-state NMR analyses of silicon and aluminum

Table 1
Properties of the parent and recrystallized H-form-ferrierite materials.

Properties		H-FER-PE	H-FER-REC
Surface area (m ² /g)	<i>S</i> _{total}	379 ± 24	406 ± 15
	<i>S</i> _{micro}	340 ± 24	248 ± 14
	<i>S</i> _{meso}	18 ± 2	76 ± 16
	<i>S</i> _{ext}	21 ± 7	82 ± 14
Pore Volume (cm ³ /g)	<i>V</i> _{total}	0.20 ± 0.02	0.38 ± 0.03
	<i>V</i> _{micro}	0.13 ± 0.01	0.10 ± 0.01
	<i>V</i> _{meso-intra}	0.01 ± 0.00	0.13 ± 0.02
	<i>V</i> _{meso-inter}	0.06 ± 0.02	0.15 ± 0.04
Si/Al		9.7 ± 0.3	6.6 ± 0.3
Total acidity (μmol/g STP)		1050 ± 31	720 ± 56

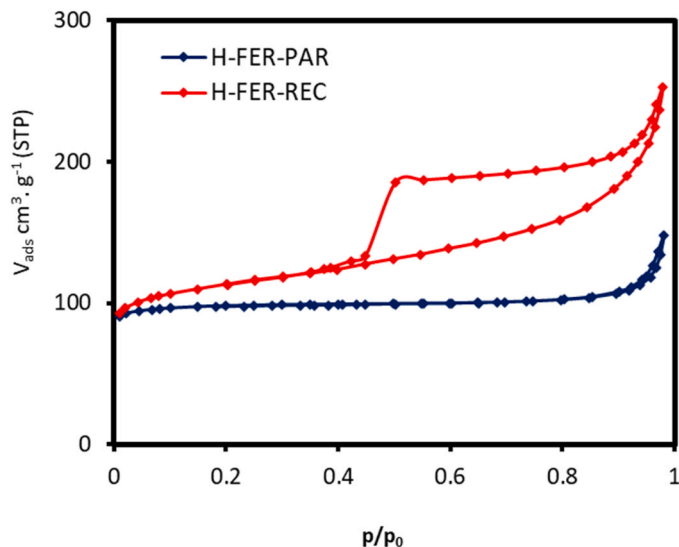


Fig. 4. N₂ sorption isotherm curves of the H-form parent and recrystallized ferrierite-based materials.

nuclei were performed on H-FER-PAR and H-FER-REC zeolitic materials.

On the one hand, by comparing the ²⁷Al MAS NMR spectra of the parent and recrystallized ferrierite (Fig S3), the following differences were observed: the region of the signal around 0 ppm associated with octahedral extra-framework aluminum (EFAL) species was increased from H-FER-PAR to H-FER-REC. In addition, the area of the signal around 55 ppm decreased between H-FER-PAR and H-FER-REC, indicating a smaller amount of tetrahedral aluminum species as part of the microporous crystalline network of the zeolite. The width of the tetrahedral Al signal increased revealing an increase in disorder in the zeolite

phase as a result of a distribution of chemical environments and/or distances. As expected, the amount of tetrahedral aluminum lost during recrystallization was proportional to the loss of acidity. In addition, the appearance of a small peak around 30 ppm showed the presence of pentahedral aluminum species associated with defects in the crystalline network of ferrierite.

By comparing the ²⁹Si MAS NMR spectra of the parent and recrystallized ferrierite (Fig S4), it was possible to see that the amount of Si sites of Q₄ type, i.e. having only Si atoms in the second coordination sphere (chemical shift (δ) at −116 ppm), does not change significantly between H-FER-PAR (22.2%) and H-FER-REC (23.0%) materials. However, the amount of Q₄-type Si atoms attached to an Al atom (δ at −111 and −106 ppm) decreased from 75.6% in H-FER-PAR to 60.7% in H-FER-REC. This clearly indicates that, despite the decreased Si/Al ratio in the solids, the fraction of Al in isostructural substitution in the zeolite network has decreased. This is consistent with the observation of Al in extra-framework octahedral species. The amount of Si sites with a chemical environment whose NMR signature appears below −106 ppm (δ at −102 and −101 ppm) increased from 2.2% in H-FER-PAR to 16.4% in H-FER-REC. These signals could be associated with Q₃ Si sites, i.e. Si atoms with an OH group in the coordination sphere. These Q₃ Si sites could be related to the formation of structural defects in the zeolite corresponding to the extraction of aluminum or an amorphous aluminosilicate phase in the sample.

In conclusion, the ²⁷Al and ²⁹Si NMR experiments revealed the presence of an Al-poor ferrierite phase in H-FER-REC coexisting with extra-framework Al-rich species. In addition, the chemical environments of Si and Al(IV) sites in the FER phase appear to be less ordered, as indicated by the increase in the linewidths.

To better understand the changes in acidity properties upon recrystallization, infrared analysis of adsorbed deuterated acetonitrile was performed on each of these materials. The use of CD₃CN, a weak base, as a surface acidity probe appears to be relevant for identifying Lewis and Brönsted acid sites and for differentiating and quantifying the strength of different Brönsted acid sites on the catalysts [48]. Fig. 6 shows the FTIR spectra of parent and recrystallized ferrierite samples before and after CD₃CN adsorption and at different temperatures during the desorption process.

The FTIR spectra of the parent and recrystallized significantly differ in the intensity of the OH stretching bands. The first band at 3746 cm^{−1} can be assigned to the ν(OH) of the terminal silanol groups (Si-OH) [44, 49,50]. The band at 3741 cm^{−1} is more intense in H-FER-REC, indicating a greater amount of terminal silanols in this material. It is expected that the silanol groups are formed during the opening of structural defects or the formation of an amorphous phase upon recrystallization. This band is consistent with the observation of more Si Q₃ sites in H-FER-REC. The band at 3660 cm^{−1} can be attributed to ν(OH) present in

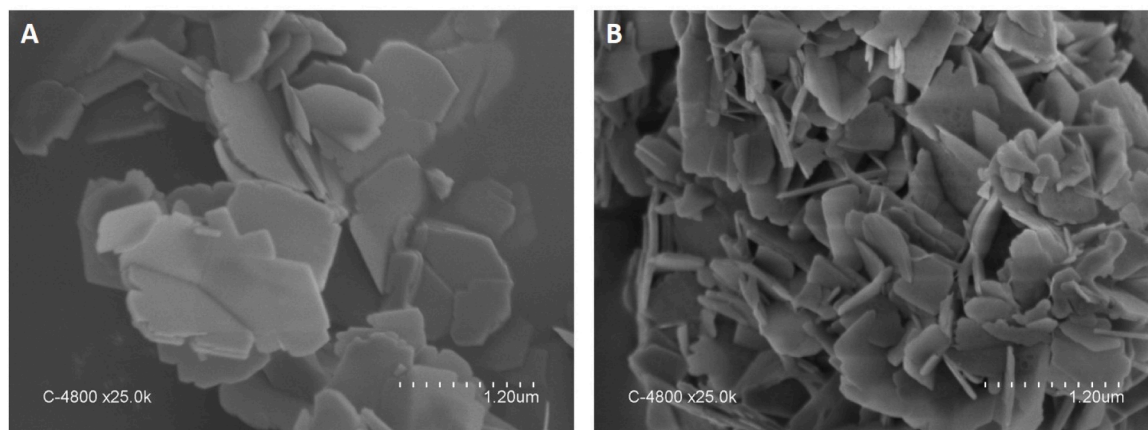


Fig. 5. SEM images of ferrierite materials with 1.2 μm scale bars. A. Parent Ferrierite (H-FER-PAR). B. Recrystallized Ferrierite (H-FER-REC).

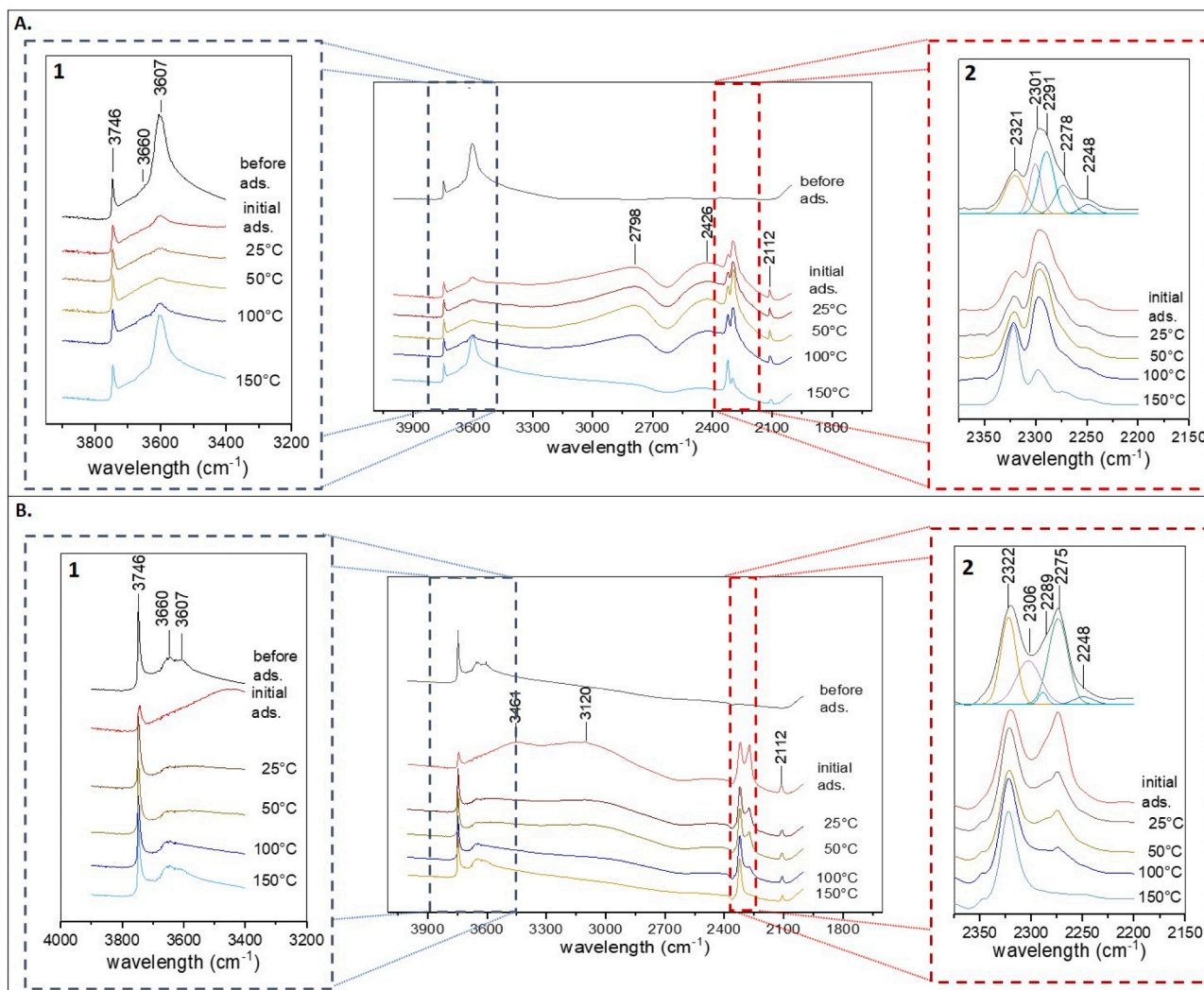


Fig. 6. FTIR spectra of CD_3CN adsorbed on ferrierite as a function of desorption temperature of (A) H-FER-PAR and (B) H-FER-REC with the enlargement of the $3400\text{--}3900\text{ cm}^{-1}$ zone (1) and the $2200\text{--}2400\text{ cm}^{-1}$ region with a model of the deconvolution procedure at initial CD_3CN adsorption (2).

extra-framework species, it is often associated in the literature with a band at 3780 cm^{-1} , characteristic of acidic OH groups bound to extra-framework aluminum, which is not observed in the present spectra [44]. The last band present in both spectra at 3607 cm^{-1} corresponds to the bridged hydroxyl groups (Si-OH-Al) on the ferrierite structure [49–51]. The band at 3607 cm^{-1} is broad and asymmetric because several types of bridging hydroxyls are present in different environments, as already shown by several studies [51,52]. The intensity of the band assigned to bridging hydroxyl groups (Si-OH-Al) is significantly lower in the recrystallized sample, which is certainly due to the loss of part of the microporous crystal framework of ferrierite during recrystallization. This is consistent with the lower amount of $\text{Q}_4(1\text{Al})$ silicon sites observed by ^{29}Si NMR.

The adsorption of CD_3CN led to a significant decrease of the terminal silanol band at 3741 cm^{-1} and to the near disappearance of the bands from 3730 to 3550 cm^{-1} corresponding to bridged hydroxyls in both samples (see Fig. 6). The disappearance of the bridged hydroxyl bands in H-FER-PAR is accompanied by the development of broad bands centered at 2798 and 2425 cm^{-1} , corresponding to Fermi resonances between the modes of vibration of the adduct of CD_3CN with strong Brönsted sites [53,54]. In the case of H-FER-REC, the decrease of the 3746 cm^{-1} signal with adsorption is accompanied by the formation of broad bands at 3464 and 3120 cm^{-1} , the first one typical of the interaction of CD_3CN with silanols and the second one generally observed on amorphous

silica-alumina, also derived from amorphisation of zeolites [54–57].

With CD_3CN adsorption, two broad bands appeared between 2400 and 2200 cm^{-1} , corresponding to the acetonitrile bands in OH-NCCD₃ molecular complexes between the bridged hydroxyl groups and the acetonitrile on the surface. These bands are typical of strong acid sites on the surface [49]. An enlargement of this region is shown in Fig. 6 for both materials. Two weak bands at 2112 and 2248 cm^{-1} , which are present throughout the CD_3CN adsorption process and are not modified by the desorption process, can be assigned to the frequencies $\nu_s(\text{CD}_3)$ and $\nu_{\text{as}}(\text{CD}_3)$. In the $\nu(\text{CN})$ spectral region, the two broad bands obtained, the first from 2350 to 2310 cm^{-1} and the second from 2310 to 2250 cm^{-1} , were assigned to Lewis and Brönsted acidic sites, based on data found in the literature [44,49,54,58,59]. These bands are composites with several components identified in both materials after deconvolution of the spectra. The band at 2278 cm^{-1} on H-FER-PAR and 2275 cm^{-1} on H-FER-REC corresponds to adsorption on silanols, which are weak Brönsted acids, in agreement with previous studies in the literature [54, 60]. The band at 2291 cm^{-1} on H-FER-PAR and 2289 cm^{-1} on H-FER-REC and the band at 2301 cm^{-1} on H-FER-PAR and 2306 cm^{-1} on H-FER-REC are attributed to the adsorption of CD_3CN adducts with acidic sites on the bridged hydroxyl groups present in the 8-MR (8-member ring) and 10-MR channels, corresponding to strong Brönsted acid sites. The band at 2321 cm^{-1} on H-FER-PAR and 2322 cm^{-1} on H-FER-REC corresponds to acetonitrile adsorbed on Lewis acidic sites [44,49,54,58,59]. The

presence of Lewis sites is frequent in ferrierite, a zeolite easily subject to dehydroxylation of Brönsted sites [61]. Comparing H-FER-PAR and H-FER-REC in the CN spectral region (Fig. 6 A and Fig. 6 B) after desorption at 25 °C, it can be seen that the ratio of Brönsted to Lewis acid sites decreases upon recrystallization; this is both a consequence of the decrease in the amount of strong Brönsted sites and the increase of the Lewis site. The formation of Lewis acid-active EFALs would be itself related to the increase in terminal silanols in H-FER-REC.

It has been observed that, in the comparison of different zeolites, the highest acid strength corresponded to the highest wavenumber of CD₃CN adsorbed on Brönsted sites [48,53,62]. Considering that the most stable Brönsted sites of ferrierite are located in the [8²6²6⁴5⁸] cavity between two 8-MRs [63], the deconvoluted band at 2291 cm⁻¹ in H-FER-PAR and 2289 cm⁻¹ in H-FER-REC was assigned to the acidic sites within the 8-MR channels while the band at 2301 cm⁻¹ in H-FER-PAR and 2306 cm⁻¹ in H-FER-REC was assigned to the acidic sites within the 10-MR channels. An interesting feature is that the relative content of the Brönsted acid sites in 8-MR decreases significantly upon recrystallization, compared to the sites in 10-MR environments. This could be related to already observed effects of recrystallization, namely the increase of silanols and Lewis sites. A local accumulation of EFAL species in the most constrained 8-MR channels would prevent the accessibility of strong Brönsted sites in the [8²6²6⁴5⁸] cavity.

Let us study the evolution of the signals as a function of the temperature of acetonitrile desorption. In the parent and recrystallized FER materials, the relative intensity of CN vibrations corresponding to bridged silanols (considering OH together in 8-MR and 10-MR) decreases less rapidly as a function of desorption temperature than the signal associated with terminal silanols. This is consistent with the higher acid strength of bridging silanols in Si-OH-Al groups.

The band deconvolution allowed us to calculate the molar density of the acid sites and thus to compare their evolution with the desorption temperature and between the two samples (Fig. 7). A larger number of total acid sites was reported on the surface of the recrystallized ferrierite immediately after adsorption of CD₃CN, mainly due to a larger amount of physisorbed CD₃CN on silanols, the weak Brönsted acid sites, at 2278 cm⁻¹. This was clearly a result of the formation of amorphous silica or defects in the zeolite framework with the desilication treatment,

which also accounted for the increase of Lewis acid EFAL in H-FER-REC. Considering the reported extinction coefficients for each type of acid site, the molar density for each site was calculated. Although there is a higher amount of weak Brönsted acid sites (silanols) in H-FER-REC (215 μmol/g) than in H-FER-PAR (101 μmol/g) at 25 °C, the ratio between them decreases significantly with desorption, indicating a very weak adsorption on the desilication-issued silanols. It is also interesting to note that the sum of Lewis and Brönsted acid sites originating from Al atoms is proportional to the variation of the Si/Al ratio in these ferrierite-based materials (H-FER-PAR: 458 μmol/g, H-FER-REC: 400 μmol/g). However, with recrystallization the number of strong Brönsted sites in 8MR decreased and virtually disappeared at higher temperature, while there was a significant increase in the amount of Brönsted acid sites from bridged hydroxyl groups in 10-MR. Preferential dealumination in 8-MR cavities and in-situ deposition of EFAL could explain both phenomena. Indeed, it has been shown that protons are extremely mobile in H-ferrierite and their location on oxygen atoms connected to Al atoms of the network is strongly dependent on the interaction with adsorbed molecules [64]. The protons of acid sites related to Al2 and Al4 sites, at the rim between 8-MR and 10-MR, if no more accessible through 8-MR could be reoriented on a neighbor oxygen and interact with CD₃CN molecules in the 10-MR.

Furthermore, as the desorption temperature was increased, the number of adsorbed CD₃CN molecules was found to be lower. This is related to its desorption from weaker acidic sites. At the highest temperature studied, 150 °C, it is noteworthy that the molar density of adsorbed molecules on Lewis acid sites is approximately similar for both materials. In contrast, the number of molecules adsorbed on Brönsted acid sites decreased with temperature. At 150 °C, it was observed that the CD₃CN molecules adsorbed on Brönsted acid sites were higher in the H-FER-PAR (131 μmol/g) than in the H-FER-REC (65 μmol/g) and no adsorption took place on 8-MR Brönsted sites. This allowed us to confirm the loss of Brönsted acid sites during the recrystallization process.

In conclusion, from the characterization of the zeolitic material obtained by one-step recrystallization of low silica ferrierite, we observe the formation of a microporous ferrierite structure with embedded mesopores. In agreement with the results obtained by Cheng *et al.* [43], this mesopore system is composed of parallelepiped mesopores with

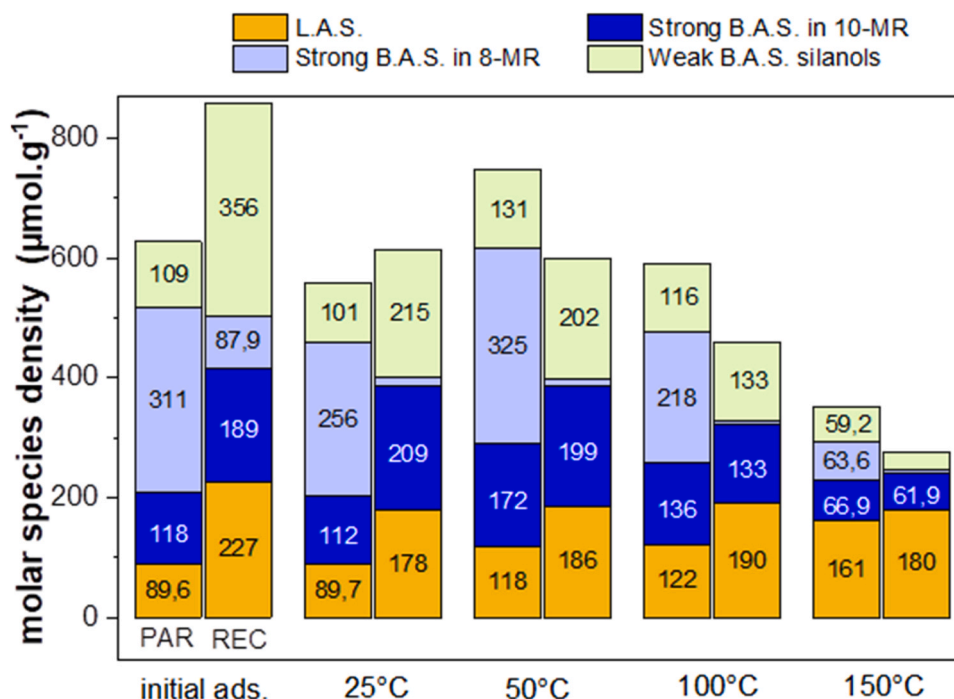


Fig. 7. Comparison of the molar density of acidic sites between parent (H-FER-PAR) and recrystallized (H-FER-REC) catalytic materials.

sizes ranging from 10 to 50 nm, which are connected to the outer surface by micropores. A loss of about a quarter of the micropore volume and about a third of the total acidity of the parent material is observed. This may be related to the dissolution of part of the ferrierite crystalline structure. Furthermore, the loss of acidity was directly proportional to the loss of tetrahedral aluminum species corresponding to the Brönsted acid sites of the ferrierite structure. In addition, the presence of a higher amount of weaker Brönsted acid sites associated with terminal silanols in H-FER-REC is certainly associated with the growth of a mesoporous phase on the zeolite crystals. This new weak Brönsted acidity is certainly not strong enough to participate in reactions requiring strong acid sites, so the new mesoporous system may simply increase the accessibility to other efficient Brönsted acid sites.

In previous studies, a secondary ordered mesoporous system or meso-microporous materials have been obtained in various ways (pillaring [65,66], transformation of larger-porosity zeolites [37], simultaneous synthesis of meso and microporous phases [67,68], synthesis of nano-stacked ferrierite crystals [69], or recrystallization processes on commercial zeolitic phases [43,70,71]) have been shown to improve diffusion, increase acid sites accessibility, and decrease catalyst deactivation rates in reactions such as 1-butene skeletal or oleic acid isomerization [37,70,72].

3.2. Catalytic Tests

The recrystallized ferrierite and its parent material have been evaluated as catalysts in methyl oleate isomerization in batch and continuous flow reactors. Various parameters such as activity, conversion, selectivity, and deactivation were evaluated.

The isomerization reaction of methyl oleate using these materials resulted in a mixture of products in the gas and liquid phases with high complexity. Different types of products are obtained due to the different reactions occurring under the studied conditions, such as isomerization, cracking, and oligomerization (Fig S5).

On the one hand, the different products present in the liquid phase were analyzed by gas chromatography. A typical liquid phase chromatogram shows the presence of monomers and oligomers (see Fig S6).

Further analysis of the monomer fraction revealed five types of compounds (see Fig S7). First, a large number of linear C_{18} mono-unsaturated fatty acid methyl esters were detected (Fig S7-i.). These types of compounds have been observed previously by Ngo et al. [73] but were not quantified as products but as intermediates [73,74]. Their identification and characterization is essential, as the position or geometry of the double bond in the methyl ester can affect their properties and applications [75]. The second group, the target of our synthesis (Fig S7-ii.) corresponds to the branched-chain C_{18} fatty acid methyl esters that result from the skeletal rearrangement of the positional and geometrical isomers of methyl oleate. The third compound observed is methyl stearate (Fig S7-iii). The fourth group (Fig S7-iv.) corresponds to lactones and the fifth group (Fig S7-v) corresponds to cracking products such as some unsaturated hydrocarbons and shorter fatty acid methyl esters that remain in the liquid fraction.

In addition, analysis of the liquid phase by MALDI-TOF (mass spectra in Fig S8) showed in addition to the previously described products, there were products corresponding to oligomers with molecular weights of 530 to 600 g/mol. Further MS-MS analysis was performed on the most intense M/Z peaks, 585.5 and 599.6 (Fig S9). The peak of $M/Z = 585.5$ broke down mainly into an ion fragment with M/Z of 303.3, representing the monomer of oleic acid, it could be assigned to dimer estolides. Then, the peak at $M/Z = 585.5$, which is fragmented into peaks with M/Z different from 303.3, could be assigned to the dimers of oleic acid.

On the other hand, GC analysis of the gas phase showed the presence of several cracking products and their derivatives. Carbon dioxide, water and methanol were also observed, as well as considerable amounts of dimethyl ether, short hydrocarbons and their isomers with carbon chain

lengths ranging from three to seven carbons. These hydrocarbons are predominantly branched and unsaturated (Fig S10).

3.2.1. Methyl oleate isomerization in a batch reactor

The first methyl oleate isomerization experiments were carried out in a batch reactor to evaluate the potential of the recrystallized ferrierite in this reaction and also to adjust the best possible reaction conditions. The first tests were carried out according to the best conditions reported in the literature for the production of isostearic acid from oleic acid, i.e. temperatures between 260 °C and 285 °C, pressures between 2 and 4 MPa and a catalyst amount of 5 wt% [15]. The results of methyl oleate isomerization are summarized in Table 2.

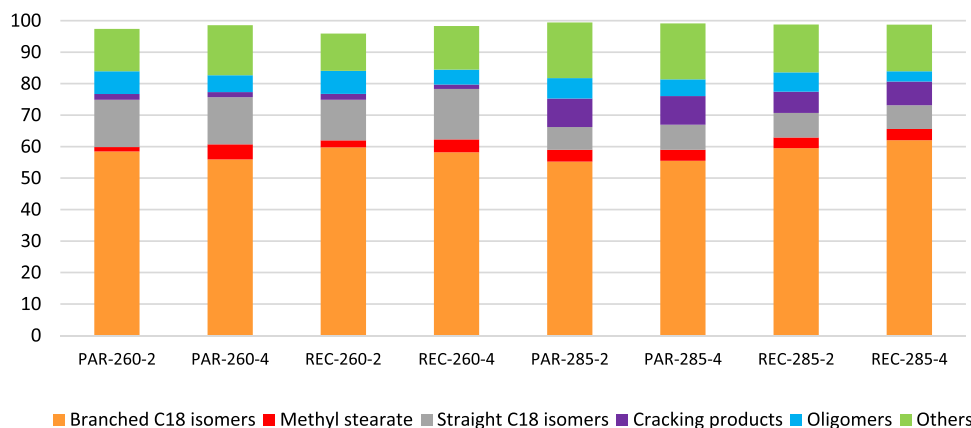
The yields in branched chain products obtained for the methyl oleate isomerization in this work under batch conditions were better than previously reported values. Fig. 8 shows the conversion and yield obtained in the methyl oleate isomerization under batch conditions. The best yield value for C_{18} branched chain products, 62.8%, was found using the recrystallized ferrierite as catalyst at 285 °C. Yields were greater than 55% in all tests. The use of ferrierite as a catalyst in this reaction was previously described. It was concluded that a ferrierite with a low Si/Al ratio and few high strength Brönsted acid sites in the 10-membered rings (10-MR) promotes the yields to branched products [74]. Although it has been described that the use of ferrierite together with some additives such as water and bulky hindered Lewis base molecules led these yields to reach values up to 80% [25,30,36,76,77], yields above 42% had not been obtained in the methyl oleate isomerization reaction [25].

In all our tests, the use of recrystallized ferrierite -H-FER-REC- showed a better yield of branched isomers compared to the parent exchanged ferrierite -H-FER-PAR. The use of H-FER-REC also brought to a slight decrease of conversion, a decrease of measured oligomerisation products and an increase of coke formation. The increase of temperature from 260 to 285 °C led to a systematic increase of conversion, decreasing of oligomerisation products and formation of more cracking products. At the highest temperature, the yield of branched products generally decreased, except when H-FER-REC was used at high N_2 pressure. The pressure of the inert gas has been generally considered having a limited influence on isomerization, albeit a slight increase of branched isomers with pressure has been observed on ferrierite and zeolite beta [23,78].

The observed effects could be mainly related to the recrystallization-induced changes in number and distribution of acid sites (Fig. 7). The effect of the greater accessibility to the micropore network on H-FER-REC compared to H-FER-PAR has also to be considered. This could lead to higher yields of branched products according to the pore mouth hypothesis [70,74]. Wiedemann et al. found that pore blockage occurs at a very early stage. It starts with the intermolecular H-transfer reactions that lead to the appearance of unsaturated carbocations, followed by the formation of cyclic conjugated ketones as precursors of alkyl benzenes [25]. It leads to the formation of highly carbonaceous materials that block the channels. As previously described for ferrierite, this first channel blockage [79] allows catalytic activity only in the acidic sites of the pore mouth of the 10-membered ring (10-MR) channels [74], which represents less than 20% of the total Brönsted acid sites in unmodified ferrierite [51]. Although the recrystallized materials have fewer strong Brönsted acid sites, as shown by FT-IR spectroscopy using acetonitrile as a probe, they present more strong Brönsted sites in 10-MR than the parent zeolite (Fig. 7). Moreover, the formation of mesopores in the recrystallization has shortened the length of the [010] 10-MR pores and led to a four-fold increase in the mesopore surface (Table 1), allowing an excellent access to the new pore mouths where the active sites are located, improving the interaction between the substrate and the internal acid sites. Although the recrystallized material -H-FER-REC- has higher amounts of other acidic sites, the weakest Brönsted acidic sites of silanols are not strong enough to participate in the isomerization reaction and also Lewis acid sites on zeolites are considered inactive in olefin

Table 2Methyl oleate isomerization conversion, selectivity, and yield in branched product values (Cat. amount: 5 wt%; reaction time: 8 h; N₂ atmosphere; batch reactor).

Temp (°C)	Catalyst	Pressure (Mpa)	Conversion (%)	Branched-chain C ₁₈ products		Coke amount in spent catalyst ^a (% wt.)
				Selectivity (%)	Yield (%)	
260	H-FER-PAR	2.0	97.4	60.0	58.4	14.5
		4.0	98.6	56.7	55.9	11.6
	H-FER-REC	2.0	95.9	62.3	59.8	19.3
		4.0	98.3	59.2	58.2	20.3
285	H-FER-PAR	2.0	99.4	55.6	55.3	13.5
		4.0	99.1	56.0	55.5	13.4
	H-FER-REC	2.0	98.8	60.2	59.5	17.9
		4.0	98.7	62.8	62.0	18.9

^a Calculated from TGA results as the sum of mass losses from 250 to 700 °C**Fig. 8.** Methyl oleate isomerization products yields obtained using H-FER-PAR and H-FER-REC as catalysts at different temperatures (260, 285 °C) and pressures (2.0, 4.0 MPa) in batch reactor for 8 h.

oligomerisation [80]. According to Wiedemann *et al.*, just the Brönsted acidic sites of high strength on the pore mouth of the 10-MR channels can carry out this reaction [74].

It can be argued if a higher diffusivity of the coke precursors due to the presence of mesopores can also play a role, despite the special geometry of the constrained mesopores of ferrierite. This could delay the deactivation of the acidic sites, allowing them to convert more molecules. It has been reported previously [41,81,82] that the formation of a mesoporous network, especially when hierarchically organized with micropores, can improve selectivity by shortening the diffusion path and avoiding secondary reactions. Although the yields of branched chain products have been improved over the commercial process using montmorillonite clay and a regeneration method has been developed [83], a fast deactivation caused by pore blockage is the main reason why this process is less economically competitive than the commercial oleic acid dimerization process [25]. Furthermore, acidic site poisoning also occurred during the isomerization reaction by strong adsorption of polyenylic species. This leads to deactivation processes of active sites at the pore mouths. Under these conditions, catalyst particles are underutilized [84], reaction rates are lower [85,86], and this coke formation [12,27] leads to faster deactivation of catalysts [87].

To gain insight into catalyst deactivation and the nature of the deactivation-causing coke, the spent catalyst materials were washed and the liquid extracts were analyzed by GC-MS and MALDI-TOF. The solid portion of the spent catalyst was analyzed by TGA to assess the amount of coke remaining on the ferrierite, and ¹³C CP MAS NMR analysis was performed to provide insight into the nature of the carbonaceous material present on the spent catalysts. The spent materials were first washed with acetone to remove residual reaction products and reactants, following the work of Wiedemann [87]. This was followed by a 24 h Soxhlet extraction with dichloromethane. This procedure removed soluble coke components that were not within the pore network of the

spent catalyst [88,89]. GC-MS and MALDI-TOF analysis of the extracted liquid phase after the first acetone wash showed that only traces of reaction products remained that were not removed after filtration. Typical MALDI-TOF spectra obtained from the liquid phase extracted with dichloromethane in the second step are shown in Fig S11. Although they showed minimal remnants of methyl oleate isomerization reaction products, the main peak obtained in all spectra of the MALDI-TOF analysis is related to alkylbenzene production intermediates ([C₁₉H₃₃O]⁺=277) previously observed in the literature as coke precursors [5,25]. This precursor was identified by MS-MS analysis at *m/z* = 277 corresponding to 1-dodecyl-6-methoxycyclohexa-1,3-diene. Methyl losses were detected in the mass spectrum corresponding to the peaks at *m/z* 269 ([C₁₈H₃₀O]Li⁺) and at *m/z* = 262 ([C₁₈H₃₀O]⁺). The peak at *m/z* = 183 of formula [C₁₂H₁₅O]Li⁺ corresponds to the loss of hexane, while the peak at *m/z* = 121 corresponds to the formula [C₈H₉O]⁺, the peak at *m/z* = 108 corresponds to methoxyphenyl [C₇H₈O]⁺ and the fragment at *m/z* = 77 is the phenyl [C₆H₅]⁺ radical, allowing us to conclude the presence of aromatic compounds in this extract.

Thermogravimetric analysis (TGA) results of the spent catalyst (Fig S12) showed three stages of mass loss previously associated with residual traces of highly volatile products (120–250 °C), residual high molecular weight products, non-polyaromatic (250–400 °C), and polyaromatic coke (400–700 °C). The amount of coke in the spent catalyst was calculated from the TGA results as the sum of the mass losses from 250 to 700 °C and the results are shown in Table 2. A higher amount of organic residues was observed in the spent catalysts derived from the recrystallized ferrierite -H-FER-REC- than in the spent catalyst derived from the parent exchanged ferrierite -H-FER-PAR-. This was observed at both temperatures studied. These higher amounts of coke can be explained by the presence of mesopores where more coke can be deposited. Although this new mesoporous network could enhance the

transport of coke precursors out of the micropore ferrierite structure, the fact that these mesopores are connected to the outer surface of the crystals by micropores could prevent these precursors from leaving the particles of the catalytic material. This is also consistent with the fact that these experiments are performed in a batch reactor (without the possibility to follow the reaction kinetics due to too many experimental hurdles), which means that the time when the maximum conversion is reached is unknown. The remaining reaction time after the maximum conversion is reached can lead to the formation of by-products and/or coke. This is likely to occur when the reactants can no longer diffuse to catalytic sites and thus can no longer be converted within the zeolite channels due to the selectivity created by the presence of the microporous channel.

To further analyze the coke, the ^{13}C CP MAS NMR spectrum of the spent catalyst was recorded to provide insight into the nature of the carbonaceous material (see Fig S13). Overall, the signals from 0 to 70 ppm were assigned to aliphatic carbons, while the signal at about 130 ppm was assigned to aromatic carbons [90–92]. Among the signals obtained between 0 and 70 ppm, the signals from 10 to 20 ppm were assigned to the methyl groups ($-\text{CH}_3$) of the aliphatic chains, while the signals from 20 to 35 ppm were assigned to the methylene groups ($-\text{CH}_2-$) of the aliphatic chains [82]. Another signal around 60 ppm was assigned to the methylene groups in the alpha or beta position on a heteroatom such as oxygen [90,92]. The primary signal of the latter group in the spent catalysts at 260 °C (spectra i and ii) could be closer to an aromatic ring, leading to a downfield shift in the spectrum. This could indicate a higher aromaticity in this spent catalyst. The same phenomenon is observed in the spectra of spent catalysts used in the reaction at 285 °C (spectra iii and iv-S13). The signal present around 60 ppm, particularly intense in spectra iii-S13, indicates the presence of oxygen in the coke. The broad peak around 130 ppm was assigned to the

carbons of the aromatic rings. More intense signals assigned to aromatic carbons can be observed in the spent catalysts of the tests at 285 °C. This could be due to greater aromatization at 285 °C. This hypothesis is confirmed by the lower intensity in these spectra of the signal around 60 ppm related to methylene close to oxygen in the experiments at 285 °C compared to those carried out at 260 °C, indicating a lower amount of this element in the coke. Although the nature of the coke was significantly affected by the conditions of pressure or temperature, a significant difference was not observed as the coke present in the spent catalysts derived from H-FER-REC and H-FER-PAR.

3.2.2. Methyl oleate isomerization in a continuous flow reactor

It has to be observed that in the batch reactor, in the absence of kinetic monitoring, the time-dependent changes in conversion and selectivity cannot be determined. In order to better understand the catalytic performance of these materials for future industrial applications, and to complement the results already obtained in a batch reactor, the methyl oleate isomerization reaction was carried out in a continuous flow reactor with a fixed bed downstream. A very recent work on methyl oleate isomerization has been reported in flow reactor using different unmodified zeolites [93]. Long-term experiments were carried out at one temperature, 290 °C, and the best performance was obtained with an H-mordenite catalyst (Si:Al ratio=20) for 48 h long tests. However, the effect introducing mesoporosity into the zeolite framework was not investigated. This type of reaction was carried out in a continuous flow reactor. These experiments allow us to evaluate the behavior and robustness of such catalytic systems. The reaction was carried out with H-FER-PAR and H-FER-REC, both at a weight hourly space velocity (W. H.S.V.) of 3.5 h^{-1} at 260 and 285 °C as well as pressures of 2.0 and 4.0 MPa, in order to have conditions comparable to those studied in batch.

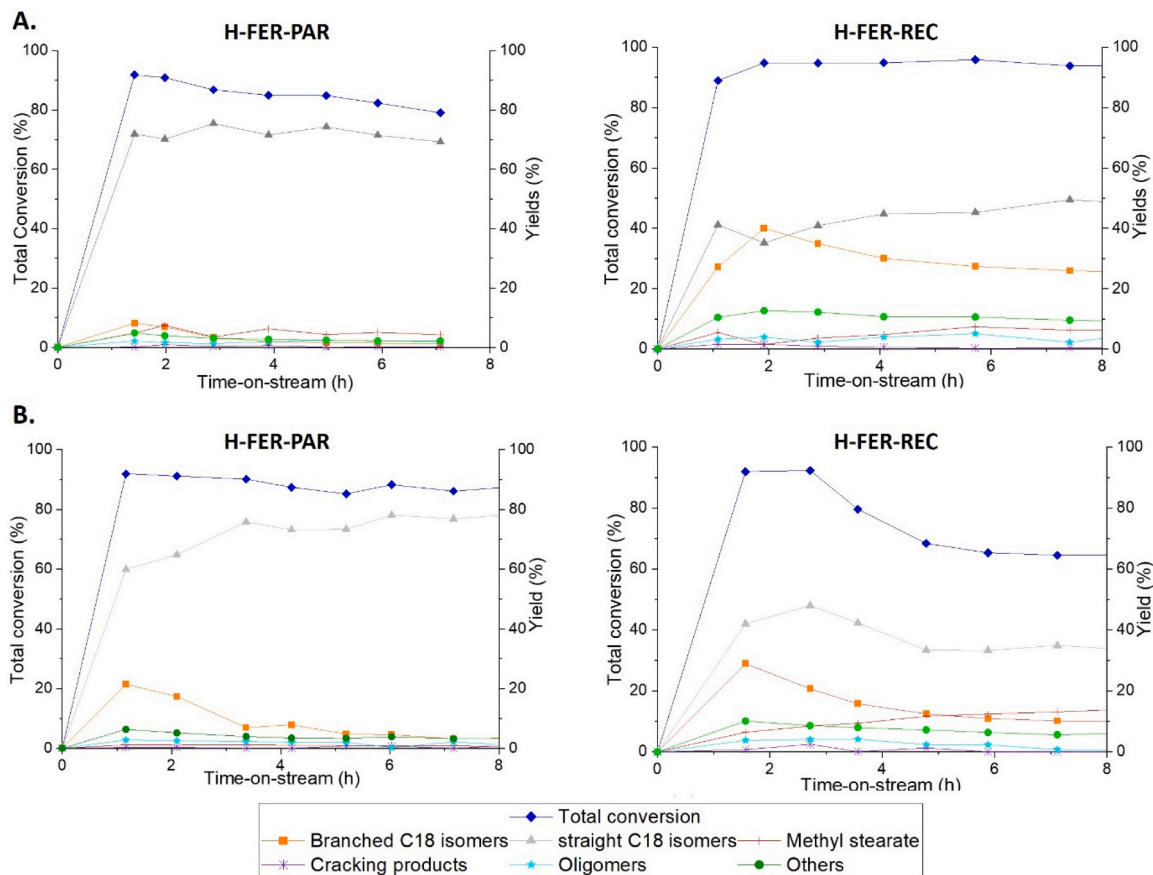


Fig. 9. Methyl oleate isomerization in a continuous flow reactor at 260 °C and pressures of A. 2.0 MPa and B. 4.0 MPa, using ferrieritic materials as catalysts.

At 260 °C and a pressure of 2.0 MPa (Fig. 9-A), the H-FER-PAR and H-FER-REC catalytic materials show similar conversion behavior, with a high and stable value over several hours and a high and fairly stable yield (with a slight increase in the case of recrystallized ferrierite) of straight C₁₈ double bond positional/geometric (cis/trans) isomers of methyl oleate with about 70% for the parent sample and about 40% for the recrystallized sample. These yield levels were not observed in the batch reactor. Regarding the yields of branched C₁₈ isomers, which are the desired products, under these pressure and temperature conditions, they were quite stable (H-FER-PAR Y_{bc}: 8.2%; H-FER-REC Y_{bc}: 40.0%) but low compared to the results obtained in batch conditions (H-FER-PAR Y_{bc}: 58.4%; H-FER-REC Y_{bc}: 59.8%) especially for the parent sample, for which the difference is huge. This behavior can be explained by a shorter contact time between the catalytic material particles and the methyl oleate compared to the batch reactor (8 h of reaction), which is not sufficient to allow consecutive reactions, generally leading to the formation of branched products. When comparing the yields of branched products using the parent and recrystallized samples, the difference is striking (about 40% with a slow decrease with time on stream for the recrystallized sample and about 8% for the parent sample), since they were almost at the same level in the batch reactor. Indeed, as shown by the FT-IR results, H-FER-rec has a higher amount of strong Brønsted acid sites in the 10-MR pores. Moreover, the contact between the methyl oleate molecules and the acidic sites present at the mouth of the 10-MR channels is favored by the high area at the surface of mesopores. Looking specifically at the results obtained with H-FER-PAR, the yields of branched chain products (8.2%) and other by-products were low. Using the parent ferrierite sample, the maximum yield (10%) was reached after one hour of time on stream and its value decreased rapidly, probably due to the deactivation of the few strong Brønsted acid sites located in the pore mouths. In contrast, using recrystallized ferrierite as a catalyst, the maximum yield of branched products (42.5%) was reached after 2 h of time on stream, and its value slowly decreased to 30%. This may be due to the new mesoporous system, which can slow down the pore blocking phenomenon by allowing the precursors of coke formation to spread from the micropore system into the mesopores. Considering that these mesopores are connected to the outer surface by micropores, when these precursors grow by oligomerization reaction, they could not leave the ferrierite particles, thus delaying the deactivation phenomena. This is confirmed by the increase in the production of by-products such as methyl stearate, lactones and oligomers, which started to increase simultaneously with the decrease in the production of branched products. At this point, due to the blockage of the internal acid sites, the catalytic activity of the external acid sites was greater, resulting in a loss of selectivity.

Looking more broadly at catalyst deactivation, shorter contact times in a flow reactor are beneficial for catalyst behavior, as conversions slowly decrease during the first few hours of reaction and then remain remarkably stable with time on stream. This is further supported by the amount of oligomers under continuous flow conditions, which decreases dramatically for both catalysts compared to batch conditions. Under these flow conditions, the short contact times probably lead to a lower probability of molecules being adsorbed on the external acidic sites, where no selectivity is observed [80].

Methyl oleate isomerization reactions were also performed at 260 °C and 4.0 MPa on H-FER-PAR and H-FER-REC (Fig. 9-B). Consistent with the previously observed behavior at 2 MPa, the major products were again the straight double bond positional/geometric isomers of methyl oleate. In the case of H-FER-PAR, the yield of straight C₁₈ isomers reached an even higher value than that obtained at 2 MPa (about 80% vs. about 70%) but the slow increase of the yield with the time-on-stream suggests that diffusional limitations are created during the reaction. The higher maximum yield of branched products (22.0%) obtained at 4.0 MPa compared to the maximum value at 2.0 MPa (8.2%) is coherent with the positive effect of carrier pressure on branching observed on several zeolites [23,78]. However, this yield decreased

rapidly after one hour of time on stream, along with the increase in straight C₁₈ isomers, probably indicating rapid deactivation of the stronger acidic sites present in the catalyst.

In the case of H-FER-REC, the conversion of methyl oleate reached 90% at the beginning of the reaction but steadily decreased after 3 h and reached 64% at 8 h time-on-stream. With longer time on stream, partial channel blockage clearly reduces catalyst performance. This can be related to the negative effect of carrier pressure on the stability of the catalyst, observed in olefin isomerization on zeolite HZSM-5 [94]. The yield of straight C₁₈ isomers reached a maximum of 40% after 3 h of time-on-stream and then decreased from 40.0% to 28.9%, together with the decrease of conversion. The maximum yield of branched products obtained with recrystallized ferrierite is still higher than in the case of the parent sample, reaching almost 30% after one hour. Then the yields of branched products decrease rapidly with time-on-stream for both parent and recrystallized samples, with a higher residual yield (10%) in the case of H-FER-REC. It appears that the increase in branching activity with pressure also favors oligomerization and byproduct formation, leading to a blockage of active sites, in a trade-off between activity and stability of the catalyst.

Finally, methyl oleate isomerization was carried out in a downstream fixed bed continuous flow at 285 °C and a pressure of 2.0 MPa for several days (Fig. 10) and showed a different behavior than at 260 °C, regardless of the pressure used. Reactions using both H-FER-PAR and H-FER-REC as catalysts showed higher conversions and yields of branched products under these conditions. Under continuous flow conditions, increasing the temperature from 260 °C to 285 °C has a significant effect. However, the rapid deactivation of the strong Brønsted acid sites and/or the rapid blocking of the micropores can be observed in the case of H-FER-PAR, as the yield of the branched product rapidly decreased from 30% to 10%, whereas it remained stable at a level of 50% in the case of H-FER-REC. The yields in lactones, oligomers and cracking products showed a similar behavior, with a maximum yield at 10% and a decrease with time on stream in the case of H-FER-PAR. These results show that increasing the temperature to 285 °C affect the catalyst stability for H-FER-PAR because it has a more constrained microporous structure in which the coke precursors accumulated more rapidly. In contrast, the positive influence of the mesoporous network in H-FER-REC is evident here, allowing better access to the acidic sites located on the 10-MR channels, leading to the stable yields of branched products observed during the first 8 h of time-on-stream. However, at this temperature, the production of oligomers increased significantly with the use of H-FER-REC, from 0.8% to 6.7% with time on stream. It has to be observed that compounds previously described in the literature as coke precursors, such as dodecylbenzene [25], which could correspond to what we obtained here, have boiling points close to 285 °C. This could increase their diffusion and thus delay the initial formation of coke affecting pore mouth catalysis. In addition, this could explain why the catalytic activity was maintained with time on stream, and why the difference in behavior between 260 °C and 285 °C is so large. It may delay the complete deactivation of the catalyst under these conditions.

In order to verify that the H-FER-REC maintains this activity for over a longer period of time and at different temperatures, the raw material flow was reduced to a WHSV of 1.2 h⁻¹ during the nights and increased back to its working value of 3.5 h⁻¹ during the day while also changing the temperature. Two higher temperatures were tested, 310 °C and 325 °C, and finally the initial temperature 285 °C was tested again to verify the condition and robustness of the catalyst after 78 h of operation (see Fig. 10).

After changing the temperature to 310 °C and taking samples again, the products obtained did not have the same composition as at 285 °C. With increasing temperature, a significant increase in oligomers, cracking products and other by-products was observed, especially on H-FER-REC catalyst. In the case of methyl oleate isomerization using H-FER-PAR (Fig. 10-A), the yield of branched products increased slightly with increasing temperature, as did the yields of lactones and oligomers.

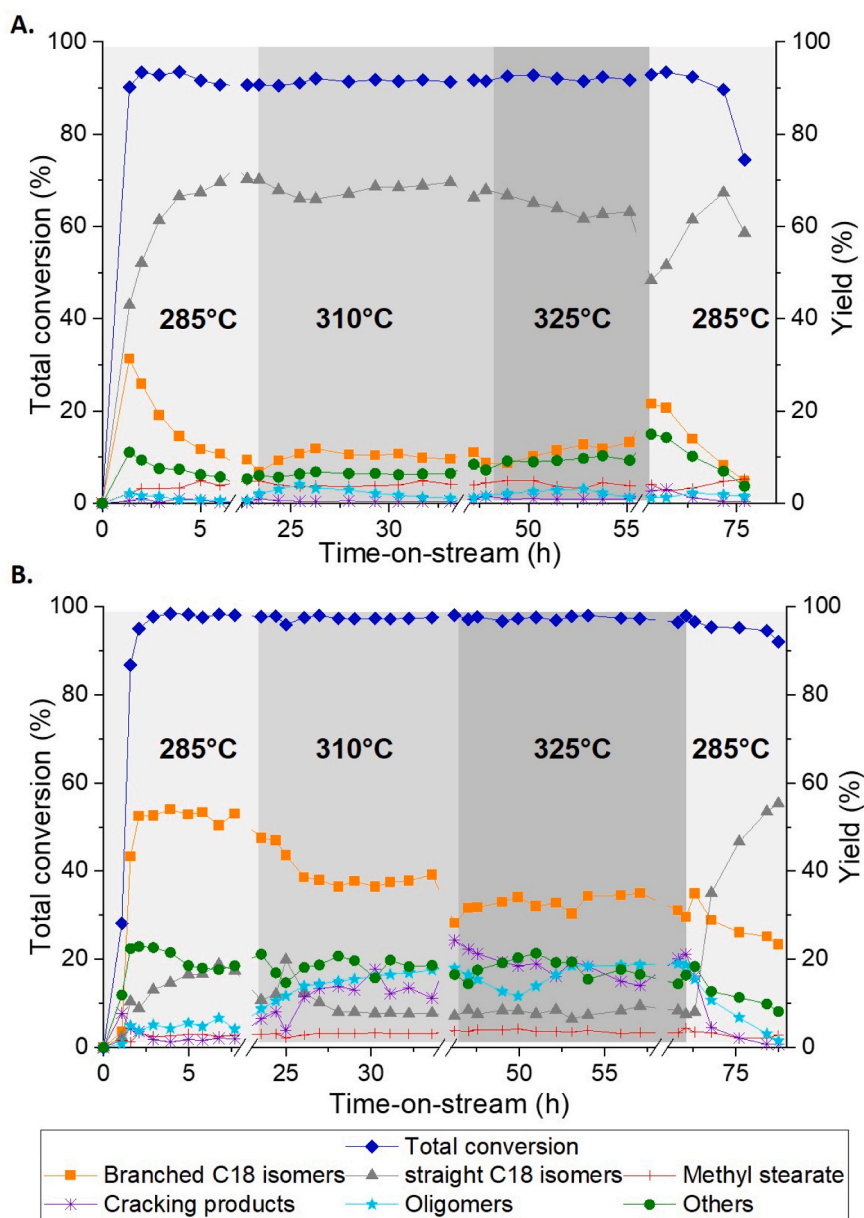


Fig. 10. Methyl oleate isomerization in a continuous flow reactor at 285, 310, and 325 °C with a return point at 285 °C at a pressure of 2.0 MPa using as the catalyst A. H-FER-PAR. B. H-FER-REC carried out for 78 h.

This increase in yield of heavier products can be explained by the increase in activity of the unblocked Brönsted acid sites with increasing temperature. However, the yields obtained were lower than those reported in the first hours of time on stream because the catalyst was already largely deactivated. On the other hand, when the reaction was carried out with H-FER-REC as catalyst (Fig. 10-B), a decrease in the yield of branched chain products was observed, while the increase in temperature led to an increase in the yield of lactones and oligomers, as well as the yield of cracking products. The higher amount of other by-products, especially oligomers and cracking products, could lead to the formation of more aromatic precursors, which could explain a lower yield of branched products as it could increase the deactivation of strong acid sites necessary for the isomerization reaction.

After the overnight period at low WHSV, the behavior of both catalysts was observed at the same temperature (310 °C). As can be seen in Fig. 10 A and B, the conversions in both cases were similar to those of the previous day, showing the stability of the catalyst with a long time on stream. Although the yield of branched products remains almost

unchanged with H-FER-PAR as catalyst, a decrease was observed in the case of H-FER-REC, accompanied by a severe increase of cracking products. This indicates that the deactivation of the H-FER-REC catalyst continues. The temperature was then raised to 325 °C. For the isomerization of methyl oleate with H-FER-PAR, the yield of branched products was quite stable, as did the yields of lactones and oligomers, but the deactivation of the catalyst continued. This indicates that the number of active Brönsted acid sites of the catalyst decreased and increasing the temperature did not help to reduce it. When H-FER-REC was used as the catalyst, the yield of branched chain products was stable with time-on-flow at the value reached with overnight lower WHSV, although this value was still higher than when the reaction is carried out with H-FER-PAR as the catalyst. Considering that the cracking reactions are favored under these temperature and pressure conditions according to what is published in the literature [27], this increase in temperature led to an increase in cracking products from 20% at 310 °C to 30% at 325 °C. The major fraction of these gaseous cracking products consisted of low molecular weight hydrocarbons and dimethyl ether. With this in mind, the

use of higher temperatures or pressures can lead to hazardous situations with increased production of volatile products. This operating temperature could also lead to an increase in the number of aromatic precursors for coke formation. This is consistent with the significant increase in the amount of oligomers observed.

The feed flow was then reduced again overnight and the temperature was changed back to 285 °C to evaluate the residual activity of the catalysts at the initial working temperature. Although the conversions were surprisingly high after the overnight period for both H-FER-PAR and H-FER-REC, both catalytic materials showed a rapid decrease with time-on-stream in activity, yields of branched products as well as other by-products. This could be probably related to strong deactivation, which should be studied in more detail.

As could be seen, increasing the temperature from 260 °C to 285 °C had a positive effect. This could be due to greater diffusion of feedstock molecules within the ferrierite framework, as well as greater diffusion of coke precursors, which increases catalytic stability and leads to higher and more stable yields of branched chain C₁₈ methyl ester products with time on stream. Although the higher temperatures of 310 and 325 °C maintained high conversions, yields of branched products decreased. In addition, these temperature increases resulted in increased cracking products and oligomer formation.

4. Conclusions

In order to obtain a ferrierite material with better performance, a mesoporous system of 10–50 nm parallelepiped internal cavities was created by one-step recrystallization using sodium hydroxide and CTAB. This procedure resulted in a hierarchical micromesoporous ferrierite H-FER-REC, with a total acidity lower than that of the parent H-FER-PAR. However, the loss of acidity was mainly due to a nearly complete passivation of Brønsted acid sites in 8-MR by extraframework species and was more than compensated by an increase of Brønsted sites accessible through 10-MR. The large mesopores created could improve the diffusivity of the reactants along the direction of the 10-MR channels and better exploit the internal acidic sites.

Under batch conditions, the use of H-FER-REC in the isomerization of methyl oleate resulted in slight improvements in yields of branched products from 58.4% to 59.8% at 260 °C and from 55.3% to 62.0% at 285 °C. Losses in selectivity typically associated with the loss of some microporosity were not observed in the experiments with H-FER-REC as catalyst because the newly formed mesopores are connected to the outer surface of the zeolite particles by micropores, which may prevent some by-products from leaving until their reconversion. The peculiar constrained mesoporosity of ferrierite allowed a four-times increase of the area of accessible [001] surfaces, providing a remarkable accessibility to the Brønsted sites at the 10-MR pore mouths. Analysis of the spent catalytic materials allowed us to observe that this mesopore system facilitates the transport of coke precursors out of the microporous framework of ferrierite and some of the coke precursors are stored in the constrained mesoporosity, delaying the effects of coking. In addition, analysis of the liquid extract of the spent catalysts allowed us to identify one of the coke precursors as 1-dodecyl-6-methoxycyclohexa-1,3-diene.

When methyl isomerization was performed in a downstream fixed bed continuous flow reactor using H-FER-REC as the catalyst, the presence of the mesopore system improved selectivity and stability of the catalyst. In addition, under continuous flow conditions, increasing the temperature from 260 °C to 285 °C had a significant effect. This could be due to a greater diffusion of feedstock molecules within the ferrierite framework and a better diffusion of coke precursors in internal mesopore reservoirs. Improvements due to the use of this micromesopore material as a catalyst and the increase in temperature to 285 °C resulted in a continuous flow process that maintained branched product yields of up to 50% with no signs of decline during the first eight hours of time on stream. To the best of our knowledge, this is the first time that the isomerization of methyl oleate has been achieved with a hierarchically

porous zeolite in a continuous flow process monitored over more than 3 days, providing valuable insight into the reaction/coking mechanism as well as catalyst behavior and deactivation.

CRediT authorship contribution statement

Tanchoux Nathalie: Conceptualization, Formal analysis, Methodology, Project administration, Supervision, Validation, Writing – review & editing. **Gérardin Corine:** Conceptualization, Formal analysis, Project administration, Supervision, Validation, Writing – review & editing, Methodology. **Riviere Maxime:** Formal analysis, Investigation. **Petit-jean Hugo:** Formal analysis, Methodology. **Di Renzo Francesco:** Formal analysis, Validation, Writing – review & editing. **Guerrero-Fajardo Carlos-Alberto:** Supervision, Validation. **Gimello Olinda:** Methodology, Writing – review & editing. **Cantor Jonathan Fabian Sierra:** Investigation, Writing – original draft.

Declaration of Competing Interest

The authors declare that they have no known competing financial interests or personal relationships that could have appeared to influence the work reported in this paper.

Data Availability

Data will be made available on request.

Acknowledgments

The authors thank the National School of Chemistry of Montpellier (ENSCM) for the financial support, and the Charles Gerhardt Institute of Montpellier (ICGM) for the technical support in this project. The authors would like to acknowledge the Chemistry Platform of Campus in Montpellier (University of Montpellier) for the support to do TEM, SEM & EDS experiments. A special acknowledgment to Emmanuel Fernandez and Philippe Gaveau for their help with the NMR analyses. The authors would like to thank Dr. Dariusz Swierczynski, Thomas Cacciaguerra, and Jeremy Rodriguez for their invaluable collaboration in the development of this project.

Appendix A. Supporting information

Supplementary data associated with this article can be found in the online version at [doi:10.1016/j.apcatb.2023.123602](https://doi.org/10.1016/j.apcatb.2023.123602).

References

- [1] J.O. Metzger, Fats and oils as renewable feedstock for chemistry, *Eur. J. Lipid Sci. Technol.* 111 (2009) 865–876, <https://doi.org/10.1002/ejlt.200900130>.
- [2] J.A. Martens, A. Bogaerts, N. De Kimpe, P.A. Jacobs, G.B. Marin, K. Rabaey, M. Saeys, S. Verhelst, The chemical route to a carbon dioxide neutral world, *ChemSusChem* 10 (2017) 1039–1055, <https://doi.org/10.1002/cssc.201601051>.
- [3] Food and Agriculture Organization of the United Nations, FAOSTAT statistical database. <https://search.library.wisc.edu/catalog/999890171702121> (accessed 27 July 2023).
- [4] R. Tesser, R. Vitiello, V. Russo, R. Turco, M. Di Serio, L. Lin, C. Li, Oleochemistry products, in: C. Li, Z. Xiao, L. He, M. Di Serio, X. Xie (Eds.), *Industrial Oil Plant*, Springer, Singapore, 2020, pp. 201–268, <https://doi.org/10.1007/978-981-15-4920-5>.
- [5] A. Masudi, O. Muraza, Vegetable oil to biolubricants: review on advanced porous catalysts, *Energy Fuels* 32 (2018) 10295–10310, <https://doi.org/10.1021/acs.energyfuels.8b02017>.
- [6] K. Hill, Fats and oils as oleochemical raw materials, *Pure Appl. Chem.* 72 (2000) 1255–1264, <https://doi.org/10.5650/jos.50.433>.
- [7] A. Bohlouli, L. Mahdavian, Catalysts used in biodiesel production: a review, *Biofuels-UK* 0 (2019) 1–14, <https://doi.org/10.1080/17597269.2018.1558836>.
- [8] A. Amin, Review of diesel production from renewable resources: catalysis, process kinetics and technologies, *Ain Shams Eng. J.* 10 (2019) 821–839, <https://doi.org/10.1016/j.asej.2019.08.001>.
- [9] S. Patnaik, S. Martha, K.M. Parida, An overview of the structural, textural and morphological modulations of g-C₃N₄ towards photocatalytic hydrogen

- production, RSC Adv. 6 (2016) 46929–46951, <https://doi.org/10.1039/C5RA26702A>.
- [10] K. Albrecht, R. Hallen, A. Brief Literature Overview of Various Routes to Renewable Fuels from Lipids for the National Alliance for Advanced Biofuels and Bio-products (NAABB) Consortium, Richland, WA: Pacific Northwest National Laboratory, 2011. <https://www.pnnl.gov/publications/brief-literature-overview-various-routes-biorenewable-fuels-lipids-national-alliance>.
 - [11] C. Renee, A novel bifunctional catalyst for alkene isomerization: development, scope and limitations, and applications in organic transformations, PhD thesis, University of California, 2012, <https://escholarship.org/uc/item/61q7f7j4>.
 - [12] A. Dhar, R.L. Vekariya, P. Bhadja, n-Alkane isomerization by catalysis—a method of industrial importance: An overview, Cogent Chem. 4 (1) (2018) 19, <https://doi.org/10.1080/23312009.2018.1514686>.
 - [13] Q. Yu, Y.-X. Ma, Z. Qin, X.-R. Luo, H.-M. Liu, X.-D. Wang, Using solid acid catalysts to improve the oxidative stability of cold-pressed sesame oil, LWT-Food Sci. Technol. 141 (2021), 110928, <https://doi.org/10.1016/j.lwt.2021.110928>.
 - [14] U. Biermann, J.O. Metzger, Synthesis of alkyl-branched fatty acids, Eur. J. Lipid Sci. Technol. 110 (2008) 805–811, <https://doi.org/10.1002/ejlt.200800033>.
 - [15] M.I. Sarker, R.J. Latona, R.A. Moreau, D. Micheroni, K.C. Jones, H.L. Ngo, Convenient and environmentally friendly production of isostearic acid with protonic forms of ammonium cationic zeolites, Eur. J. Lipid Sci. Technol. 119 (2017), 1700262, <https://doi.org/10.1002/ejlt.201700262>.
 - [16] S.C.C. Wiedemann, P.C.A. Bruijninx, B.M. Weckhuysen, Isostearic acid: a unique fatty acid with great potential, in: F. Cavani, S. Albonetti, F. Basile, A. Gandini (Eds.), Chemicals and Fuels from Bio-Based Building Blocks, Wiley-VCH, Weinheim, 2016, pp. 51–78, <https://doi.org/10.1002/9783527698202.ch3>.
 - [17] U. Biermann, U.T. Bornscheuer, I. Feussner, M.A.R. Meier, J.O. Metzger, Fatty acids and their derivatives as renewable platform molecules for the chemical industry, Angew. Chem. -Int. Ed. 60 (2021) 20144–20165, <https://doi.org/10.1002/anie.202100778>.
 - [18] G. Dabrowski, I. Konopka, Update on food sources and biological activity of odd-chain, branched and cyclic fatty acids — a review, Trends Food Sci. Technol. 119 (2022) 514–529, <https://doi.org/10.1016/j.tifs.2021.12.019>.
 - [19] G. Biresaw, H.L. Ngo, R.O. Dunn, Investigation of the physical and tribological properties of iso-oleic acid, JAOCS, J. Am. Oil Chem. Soc. 96 (2019) 189–199, <https://doi.org/10.1002/aocs.12177>.
 - [20] J. Habelberg, A. Behr, Saturated branched fatty compounds: proven industrial processes and new alternatives, Eur. J. Lipid Sci. Technol. 118 (2016) 36–46, <https://doi.org/10.1002/ejlt.201500461>.
 - [21] H.L. Ngo, A. Nuñez, W. Lin, T. a Foglia, A. Nunez, W. Lin, T. a Foglia, Zeolite-catalyzed isomerization of oleic acid to branched-chain isomers, Eur. J. Lipid Sci. Technol. 109 (2007) 214–224, <https://doi.org/10.1002/ejlt.200600246>.
 - [22] R.O. Dunn, H.L. Ngo, M.J. Haas, Branched-chain fatty acid methyl esters as cold flow improvers for biodiesel, J. Am. Oil Chem. Soc. 92 (2015) 853–869, <https://doi.org/10.1007/s11746-015-2643-2>.
 - [23] S.J. Reaume, N. Ellis, Optimizing reaction conditions for the isomerization of fatty acids and fatty acid methyl esters to their branch chain products, J. Am. Oil Chem. Soc. 88 (2011) 661–671, <https://doi.org/10.1007/s11746-010-1718-3>.
 - [24] J.F. Sierra-Cantor, C.A. Guerrero-Fajardo, Methods for improving the cold flow properties of biodiesel with high saturated fatty acids content: a review, Renew. Sust. Energ. Rev. 72 (2017) 774–790, <https://doi.org/10.1016/j.rser.2017.01.077>.
 - [25] S.C.C. Wiedemann, J.A. Stewart, F. Soulimani, T. Van Bergen-Brenkman, S. Langelaar, B. Wels, P. De Peinder, P.C.A. Bruijninx, B.M. Weckhuysen, Skeletal isomerisation of oleic acid over ferrierite in the presence and absence of triphenylphosphine: pore mouth catalysis and related deactivation mechanisms, J. Catal. 316 (2014) 24–35, <https://doi.org/10.1016/j.jcat.2014.04.018>.
 - [26] G. Biresaw, Y. Chen, L. Chen, H. Ngo, K.E. Vermillion, S.C. Cermak, Iso-oleic estolide products with superior cold flow properties, Ind. Crop. Prod. 182 (2022), 114857, <https://doi.org/10.1016/j.indcrop.2022.114857>.
 - [27] J. Weitkamp, Catalytic hydrocracking-mechanisms and versatility of the process, ChemCatChem 4 (2012) 292–306, <https://doi.org/10.1002/cctc.201100315>.
 - [28] R. Maghrebi, M. Buffi, P. Bondioli, D. Chiaramonti, Isomerization of long-chain fatty acids and long-chain hydrocarbons: a review, Renew. Sust. Energ. Rev. 149 (2021), 111264, <https://doi.org/10.1016/j.rser.2021.111264>.
 - [29] A.F. Elsasser, L.A. McCargar, Method of preparing dimeric fatty acids and/or esters thereof containing low residual interesters and the resulting dimeric fatty acids and/or dimeric fatty esters, patent WO0109066, 8 Feb 2001.
 - [30] M.I. Sarker, R.A. Moreau, H.L. Ngo, Comparison of various phosphine additives in zeolite based catalytic isomerization of oleic acid, Eur. J. Lipid Sci. Technol. (2018), <https://doi.org/10.1002/ejlt.201800070>.
 - [31] H.L. Ngo, E. Hoh, T. a Foglia, Improved synthesis and characterization of saturated branched-chain fatty acid isomers, Eur. J. Lipid Sci. Technol. 114 (2012) 213–221, <https://doi.org/10.1002/ejlt.201000471>.
 - [32] J.C. Yori, M.A. D'Amato, J.M. Grau, C.L. Pieck, C.R. Vera, Depression of the cloud point of biodiesel by reaction over solid acids, Energy Fuels 20 (2006) 2721–2726, <https://doi.org/10.1021/ef060245i>.
 - [33] W.R. Hodgson, W. Tijmen, C. Lok, G. Roberts, Fatty acid isomerisation, patent US005856539A, 5 Jan 1999.
 - [34] L. Ha, J. Mao, J. Zhou, Z.C. Zhang, S. Zhang, Skeletal isomerization of unsaturated fatty acids on Beta zeolites: effects of calcination temperature and additives, Appl. Catal. A-Gen. 356 (2009) 52–56, <https://doi.org/10.1016/j.apcata.2008.12.018>.
 - [35] S. Zhang, Z. Zhang, D. Steichen, Skeletal Isomerization of Fatty Acids, patent US2003100780, 29 May 2003.
 - [36] J. Zhang, J. Uknalis, L. Chen, R.A. Moreau, H.L. Ngo, Development of magnesium oxide-zeolite catalysts for isomerization of fatty acids, Catal. Lett. 149 (2019) 303–312, <https://doi.org/10.1007/s10562-018-2601-3>.
 - [37] A. Bolshakov, R. van de Poll, T. van Bergen-Brenkman, S.C.C. Wiedemann, N. Kosinov, E.J.M. Hensen, Hierarchically porous FER zeolite obtained via FAU transformation for fatty acid isomerization, Appl. Catal. B-Environ. 263 (2019), 118356, <https://doi.org/10.1016/j.apcatb.2019.118356>.
 - [38] S. Zhang, Z.C. Zhang, Skeletal isomerization of unsaturated fatty acids: the role of mesopores in HBeta zeolites, Catal. Lett. 115 (2007) 114–121, <https://doi.org/10.1007/s10562-007-9083-z>.
 - [39] S. Mardiana, J.A. Azhari, G.T.M. Kadja, On the effectiveness of hierarchical zeolite catalyst for isomerization of biomass-derived compound, J. Res. Dev. Nanotechnol. 1 (2021) 23–27, <https://doi.org/10.5614/jrdn.2021.1.1.16619>.
 - [40] D. Kerstens, H. De Puter, I. Khalil, S. Van Praet, J. Van Aelst, B.F. Sels, Fast and selective solvent-free branching of unsaturated fatty acids with hierarchical ZSM-5, ACS Sustain. Chem. Eng. 9 (2021) 4357–4362, <https://doi.org/10.1021/acscuschemeng.0c09161>.
 - [41] J. García-Martínez, K. Li, Mesoporous Zeolites: Preparation, Characterization, and Applications, Wiley-VCH, Weinheim, 2015, <https://doi.org/10.1002/9783527673957>.
 - [42] D. Verboekend, N. Nuttens, R. Locu, J. Van Aelst, P. Verolme, J.C. Groen, J. Pérez-Ramírez, B.F. Sels, Synthesis, characterisation, and catalytic evaluation of hierarchical faujasite zeolites: milestones, challenges, and future directions, Chem. Soc. Rev. 45 (2016) 3331–3352, <https://doi.org/10.1039/c5cs00520e>.
 - [43] X. Cheng, T. Cacciaguerra, D. Minoux, J.P. Dath, F. Fajula, C. Gérardin, Generation of parallelpiped-shaped mesopores and structure transformation in highly stable ferrierite zeolite crystals by framework desilication in NaOH solution, Micro Mesopor. Mat. 260 (2018) 132–145, <https://doi.org/10.1016/j.micromeso.2017.05.050>.
 - [44] B. Gil, S.I. Zones, S.J. Hwang, M. Bejblova, J. Čejka, Acidic properties of SSZ-33 and SSZ-35 novel zeolites: a complex infrared and MAS NMR study, J. Phys. Chem. C. 112 (2008) 2997–3007, <https://doi.org/10.1021/jp077687v>.
 - [45] I.I. Ivanova, I.A. Kasyanov, A.A. Maerle, V.I. Zaikovskii, Mechanistic study of zeolites recrystallization into micro-mesoporous materials, Microporous Mesoporous Mat. 189 (2014) 163–172, <https://doi.org/10.1016/j.micromeso.2013.11.001>.
 - [46] A. Sachse, A. Grau-Artienza, E.O. Jardim, N. Linares, M. Thommes, J. García-Martínez, Development of intracrystalline mesoporosity in zeolites through surfactant-templating, Cryst. Growth Des. 17 (2017) 4289–4305, <https://doi.org/10.1021/acs.cgd.7b00619>.
 - [47] I.I. Ivanova, E.E. Knyazeva, Micro-mesoporous materials obtained by zeolite recrystallization: synthesis, characterization and catalytic applications, Chem. Soc. Rev. 42 (2013) 3671–3688, <https://doi.org/10.1039/c2cs35341e>.
 - [48] A.G. Pelmentschikov, R.A. Van Santen, J. Jänchen, E. Meijer, CD3CN as a probe of lewis and bronsted acidity of zeolites, J. Phys. Chem. 97 (1993) 11071–11074, <https://doi.org/10.1021/j100144a028>.
 - [49] T.M. Davis, C.Y. Chen, N. Žilková, D. Vitvarová-Procházková, J. Čejka, S.I. Zones, The importance of channel intersections in the catalytic performance of high silica stilbite, J. Catal. 298 (2013) 84–93, <https://doi.org/10.1016/j.jcat.2012.10.022>.
 - [50] R. Rachwalik, M. Hunger, B. Sulikowski, Transformations of monoterpene hydrocarbons on ferrierite type zeolites, Appl. Catal. A-Gen. 427–428 (2012) 98–105, <https://doi.org/10.1016/j.apcata.2012.03.037>.
 - [51] V.L. Zholobenko, D.B. Lukyanov, J. Dwyer, W.J. Smith, Ferrierite and SUZ-4 zeolite: characterization of acid sites, J. Phys. Chem. B 102 (1998) 2715–2721, <https://doi.org/10.1021/jp973340o>.
 - [52] K. Chakarova, K. Hadjiivanov, FTIR study of N₂ and CO adsorption on H-D-FER, Microporous Mesoporous Mater. 177 (2013) 59–65, <https://doi.org/10.1016/j.micromeso.2013.04.022>.
 - [53] S. Bordiga, C. Lamberti, F. Bonino, A. Travert, F. Thibault-Starzyk, Probing zeolites by vibrational spectroscopies, Chem. Soc. Rev. 44 (2015) 7262–7341, <https://doi.org/10.1039/c5cs00396b>.
 - [54] C. Pazé, A. Zecchina, S. Spera, G. Spano, F. Rivetti, Acetonitrile as probe molecule for an integrated ¹H NMR and FTIR study of zeolitic Bronsted acidity: Interaction with zeolites H-ferrierite and H-beta, Phys. Chem. Chem. Phys. 2 (2000) 5756–5760, <https://doi.org/10.1039/B0056770>.
 - [55] P.G. Rouxhet, R.E. Sempels, Hydrogen bond strengths and acidities of hydroxyl groups on silica-alumina surfaces and in molecules in solution, J. Chem. Soc. Faraday Trans. 170 (1974) 2021–2032, <https://doi.org/10.1039/F1974000201>.
 - [56] R.E. Sempel, P.G. Rouxhet, Infrared study of the adsorption of benzene and acetonitrile on silica-alumina gels: acidity properties and surface heterogeneity, J. Colloid Interface Sci. 55 (1976) 263–273, [https://doi.org/10.1016/0021-9797\(76\)90033-3](https://doi.org/10.1016/0021-9797(76)90033-3).
 - [57] W. Daniell, N.Y. Topsøe, H. Knözinger, An FTIR study of the surface acidity of USY zeolites: Comparison of CO, CD₃CN, and C₆H₅N probe molecules, Langmuir 17 (2001) 6233–6239, <https://doi.org/10.1021/la010345a>.
 - [58] R. Rachwalik, Z. Olejniczak, B. Sulikowski, Dealumination of ferrierite type zeolite: physicochemical and catalytic properties, Catal. Today 101 (2005) 147–154, <https://doi.org/10.1016/j.cattod.2005.01.012>.
 - [59] E. Catizzone, M. Miglioni, T. Mineva, S. van Daele, V. Valtchev, G. Giordano, New synthesis routes and catalytic applications of ferrierite crystals. Part 2: The effect of OSDA type on zeolite properties and catalysis, Microporous Mesoporous Mat. 296 (2020), 109988, <https://doi.org/10.1016/j.micromeso.2019.109988>.
 - [60] A.A. Belhekar, R.K. Ahedi, S. Kuriyavar, S.S. Shevade, S.S. Rao, R. Anand, Z. Tvaruzkova, Effect of acid sites of Al- and Fe-Ferrierite on m-xylene isomerization, Commun. Commun. 4 (2003) 295–302, [https://doi.org/10.1016/S1566-7367\(03\)00056-6](https://doi.org/10.1016/S1566-7367(03)00056-6).
 - [61] B. Wichterlova, Z. Tvaruzkova, Z. Sobalik, P. Sarv, Determination and properties of acid sites in H-ferrierite. A comparison of ferrierite and MFI structures,

- Microporous Mesoporous Mat. 24 (1998) 223–233, [https://doi.org/10.1016/S1387-1811\(98\)00167-X](https://doi.org/10.1016/S1387-1811(98)00167-X).
- [62] L. Kubelková, J. Kotrla, J. Florián, H-bonding and interaction energy of acetonitrile neutral and pyridine ion-pair surface complexes in zeolites of various acidity: FTIR and ab initio study, *J. Phys. Chem.* 99 (1995) 10285–10293, <https://doi.org/10.1021/j100025a033>.
- [63] M. Rubes, M. Trachta, J. Vaculík, R. Bulanek, O. Bludský, The analysis of the BAS OH band in zeolites, *Micro Mesopor. Mat.* 341 (2022), 112052, <https://doi.org/10.1016/j.micromeso.2022.112052>.
- [64] A. Alberti, A. Martucci, Proton transfer mediated by water: experimental evidence by neutron diffraction, *J. Phys. Chem. C* 114 (2010) 7767–7773, <https://doi.org/10.1021/jp100370u>.
- [65] E.G. Fuentes-Ordóñez, J.A. Salbidegoitia, J.L. Ayastuy, M.A. Gutiérrez-Ortiz, M. P. González-Marcos, J.R. González-Velasco, High external surface Pt/zeolite catalysts for improving polystyrene hydrocracking, *Catal. Today* 227 (2014) 163–170, <https://doi.org/10.1016/j.cattod.2013.09.004>.
- [66] W.J. Roth, B. Gil, A. Mayoral, J. Grzybek, A. Korzeniowska, M. Kubu, W. Makowski, J. Čejka, Z. Olejniczak, M. Mazur, Pillaring of layered zeolite precursors with ferrierite topology leading to unusual molecular sieves on the micro/mesoporous border, *Dalton Trans.* 47 (2018) 3029–3037, <https://doi.org/10.1039/c7dt03718j>.
- [67] X. Niu, Y. Song, S. Xie, S. Liu, Q. Wang, L. Xu, Synthesis and catalytic reactivity of MCM-22/ZSM-35 composites for olefin aromatization, *Catal. Lett.* 103 (2005) 211–218, <https://doi.org/10.1007/s10562-005-7156-4>.
- [68] S. Xie, S. Liu, Y. Liu, X. Li, W. Zhang, L. Xu, Synthesis and characterization of MCM-49/ZSM-35 composite zeolites in the hexamethyleneimine and cyclohexamine system, *Microporous Mesoporous Mat.* 121 (2009) 166–172, <https://doi.org/10.1016/j.micromeso.2009.01.027>.
- [69] E. Koohsaryan, M. Anbia, Nanosized and hierarchical zeolites: a short review, *Chin. J. Catal.* 37 (2016) 447–467, [https://doi.org/10.1016/S1872-2067\(15\)61038-5](https://doi.org/10.1016/S1872-2067(15)61038-5).
- [70] Y.P. Khiteev, Y.G. Kolyagin, I.I. Ivanova, O.A. Ponomareva, F. Thibault-Starzyk, J.-P. Gilson, C. Fernandez, F. Fajula, Synthesis and catalytic properties of hierarchical micro/mesoporous materials based on FER zeolite, *Microporous Mesoporous Mat.* 146 (2011) 201–207, <https://doi.org/10.1016/j.micromeso.2011.05.003>.
- [71] D. Li, Y. Chen, J. Hu, B. Deng, X. Cheng, Y. Zhang, Synthesis of Hierarchical Chabazite Zeolite via Interzeolite Transformation of Coke-containing Spent MFI, *Appl. Catal. B-Environ.* 270 (2020), 118881, <https://doi.org/10.1016/j.apcatb.2020.118881>.
- [72] Y.P. Khiteev, I.I. Ivanova, Y.G. Kolyagin, O.A. Ponomareva, Skeletal isomerization of 1-butene over micro/mesoporous materials based on FER zeolite, *Appl. Catal. A-Gen.* 441–442 (2012) 124–135, <https://doi.org/10.1016/j.apcata.2012.07.010>.
- [73] H.L. Ngo, R.O. Dunn, E. Hoh, C₁₈-unsaturated branched-chain fatty acid isomers: characterization and physical properties, *Eur. J. Lipid Sci. Technol.* 115 (2013) 676–683, <https://doi.org/10.1002/ejlt.201200323>.
- [74] S.C.C. Wiedemann, A. Muñoz-Murillo, R. Oord, T. Van Bergen-Brenkman, B. Wels, P.C. a Bruijninx, B.M. Weckhuysen, Skeletal isomerisation of oleic acid over ferrierite: Influence of acid site number, accessibility and strength on activity and selectivity, *J. Catal.* 329 (2015) 195–205, <https://doi.org/10.1016/j.jcat.2015.05.013>.
- [75] G. Knothe, R.O. Dunn, A comprehensive evaluation of the melting points of fatty acids and esters determined by differential scanning calorimetry, *J. Am. Oil Chem. Soc.* 86 (2009) 843–856, <https://doi.org/10.1007/s11746-009-1423-2>.
- [76] H.L. Ngo, Lewis base additives improve the zeolite Ferrierite-catalyzed synthesis of isostearic acids synthesis of isostearic acids, *J. Am. Oil Chem. Soc.* 92 (2015) 613–619, <https://doi.org/10.1007/s11746-015-2608-5>.
- [77] M. Fan, T. Si, P. Zhang, Effect of surface modification of H⁺-mordenite on the isomerization of oleic acid into branched-chain isomers, *J. Am. Oil Chem. Soc.* 95 (2018) 1357–1365, <https://doi.org/10.1002/aocs.12142>.
- [78] A. Ferreira Young, P. Nothaft Romano, J. Monnerat Araújo Ribeiro de Almeida, D. A. Gomes Aranda, Isomerization of oleic acid over acid zeolites: design of experiments and proposal of a novel kinetic mechanism, *Ind. Eng. Chem. Res.* 60 (2021) 14051–14059, <https://doi.org/10.1021/acs.iecr.1c02054>.
- [79] S.C.C. Wiedemann, Z. Ristanović, G.T. Whiting, V.R. Reddy Marthala, J. Kärger, J. Weitkamp, B. Wels, P.C.A. Bruijninx, B.M. Weckhuysen, Large ferrierite crystals as models for catalyst deactivation during skeletal isomerisation of oleic acid: evidence for pore mouth catalysis, *Chem. -Eur. J.* 22 (2016) 199–210, <https://doi.org/10.1002/chem.201503551>.
- [80] J. Houzvíčka, V. Ponec, Skeletal isomerisation of n-butene on phosphorus containing catalysts, *Appl. Catal. A: Gen.* 145 (1996) 95–109, [https://doi.org/10.1016/0926-860X\(96\)00144-5](https://doi.org/10.1016/0926-860X(96)00144-5).
- [81] R. Chal, C. Gerardin, M. Bulut, S. Van Donk, Overview and industrial assessment of synthesis strategies towards zeolites with mesopores, *ChemCatChem* 3 (2011) 67–81, <https://doi.org/10.1002/cctc.201000158>.
- [82] R. Srivastava, Synthesis and applications of ordered and disordered mesoporous zeolites: present and future prospective, *Catal. Today* 309 (2018) 172–188, <https://doi.org/10.1016/j.cattod.2017.08.017>.
- [83] H.L. Ngo, T.A. Foglia, Process for preparing saturated branched chained fatty acids, patent US2011275844, 10 Nov 2011.
- [84] D. Verboekend, New Hierarchical Zeolite Catalysts by Post-Synthetic Design, PhD thesis, ETH Zurich, 2012. <https://doi.org/10.3929/ethz-a-007595445>.
- [85] L. Vaugon, Etude des performances en hydrocraquage de catalyseurs zéolithiques modèles: influence de l'architecture poreuse et de l'acidité, PhD thesis, ENSCM, Montpellier, 2017. <https://www.theses.fr/2017ENCM0015>.
- [86] S. Van Donk, Adsorption, Diffusion and Reaction Studies of Hydrocarbons on Zeolite Catalysts, PhD thesis Utrecht university, 2002. <https://dspace.library.uu.nl/handle/1874/764>.
- [87] S.C.C. Wiedemann, Ferrierite-Catalysed Branching of Unsaturated Fatty Acids, PhD thesis, Utrecht University, 2015. <https://dspace.library.uu.nl/handle/1874/324940>.
- [88] S. Hamieh, Transformation des alcools sur zéolithes protoniques: "rôle paradoxal du coke", PhD thesis, University of Poitiers, 2013. <http://nuxeo.edel.univ-poitiers.fr/nuxeo/site/esupversions/c9b0cca1-c5f5-4304-98b6-10e76e998104>.
- [89] H.S. Cerqueira, C. Sievers, G. Joly, P. Magnoux, J.A. Lercher, Multitechnique characterization of coke produced during commercial resid FCC operation, *Ind. Eng. Chem. Res.* 44 (2005) 2069–2077, <https://doi.org/10.1021/ie048963k>.
- [90] C.E. Snape, B.J. McGhee, S.C. Martin, J.M. Andresen, Structural characterisation of catalytic coke by solid-state ¹³C NMR spectroscopy, *Catal. Today* 37 (1997) 285–293, [https://doi.org/10.1016/S0926-5861\(97\)00021-7](https://doi.org/10.1016/S0926-5861(97)00021-7).
- [91] M.A. Callejas, M.T. Martínez, T. Blasco, E. Sastre, Coke characterisation in aged residue hydrotreating catalysts by solid-state ¹³C NMR spectroscopy and temperature-programmed oxidation, *Appl. Catal. A-Gen.* 218 (2001) 181–188, [https://doi.org/10.1016/S0926-860X\(01\)00640-8](https://doi.org/10.1016/S0926-860X(01)00640-8).
- [92] A. Devaraj, M. Vijayakumar, J. Bao, M.F. Guo, M.A. Derewinski, Z. Xu, M.J. Gray, S. Proding, K.K. Ramasamy, Discerning the location and nature of coke deposition from surface to bulk of spent zeolite catalysts, 2016, *Sci. Rep.* 6 (2016), 37586, <https://doi.org/10.1038/srep37586>.
- [93] M. Kondratiuk, D. Gopinath, A. Elrrays, L.J. Gooßen, Double-bond isomerization of rapeseed oil methyl esters in a continuous flow reactor efficiently catalyzed by H-mordenite, *Eur. J. Lipid Sci. Technol.* 125 (2023), 2200163, <https://doi.org/10.1002/ejlt.202200163>.
- [94] M. Díaz, E. Epelde, A.T. Aguayo, J. Bilbao, Low-pressure oligomerization of 1-butene to liquid fuels on HZSM-5. zeolite catalysts: effect of operating conditions, *J. Ind. Eng. Chem.* 87 (2020) 234–241, <https://doi.org/10.1016/j.jiec.2020.04.006>.